REVIEW

National Science Open
3: 20230056, 2024
https://doi.org/10.1360/nso/20230056

Engineering

Special Topic: Energy Systems of Low Carbon Buildings

Advancements and challenges in enhancing salt hydrate phase change materials for building energy storage: Optimization methodologies and mechanisms

Haibin Yang[#], Yang Zou[#] & Hongzhi Cui[*]

Key Laboratory for Resilient Infrastructures of Coastal Cities (Ministry of Education), College of Civil and Transportation Engineering, Shenzhen University, Shenzhen 518060, China

#The authors contributed equally to this work.
*Corresponding author (email: h.z.cui@szu.edu.cn)

Received 7 September 2023; Revised 22 November 2023; Accepted 8 January 2024; Published online 9 January 2024

Abstract: The application of phase change materials (PCMs) into buildings is a prospective method for mitigating energy consumption in the construction sector. Among the diverse PCM options, salt hydrate PCMs stand out for their superior thermal storage densities, adaptable operating temperature ranges, and cost-effectiveness, rendering them highly attractive for practical engineering applications. However, the utilization of salt hydrates has encountered obstacles, including pronounced supercooling, severe phase separation, and insufficient thermal conductivity, limiting their efficacy in energy storage solutions. In response to these challenges and in pursuit of rendering salt hydrates viable for building energy storage systems, substantial research has been conducted in recent years. This paper offers a comprehensive overview of the strategies devised to address the challenges associated with salt hydrate PCMs, and it also elucidates the corresponding optimization methodologies and bolstering mechanisms, providing a valuable resource for researchers in this field.

Keywords: salt hydrates, phase change materials, supercooling degree, phase separation, thermal conductivity, corrosion behavior

INTRODUCTION

Addressing climate change is a major challenge worldwide. Building energy consumption is a significant contributor to global energy consumption and CO_2 emissions, with approximately 50% of this demand attributed to thermal energy requirements, notably space heating and domestic water supply. As demonstrated in Figure 1A, cities in Northern China exhibit exceptionally high annual heating demands, with over 54.9% of them having annual heating intensities exceeding 100 kWh/(m^2 a) [1]. Moreover, at the national level, the total CO_2 emissions from centralized building heating maintained an increasing trend [2], with per capita CO_2 emissions from space heating and domestic water heating accounting for a substantial 78% of the total emissions [3], as shown in Figure 1B and C.

The pursuit of reduced building energy consumption has spurred extensive research into phase change

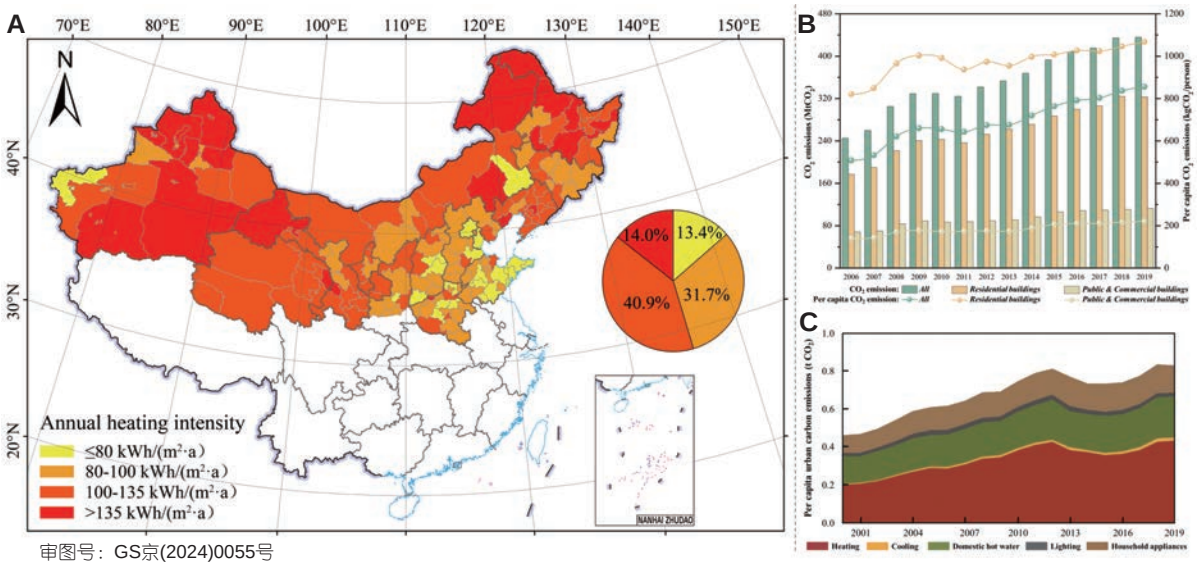

Figure 1 Thermal energy demand in China. (A) Annual heating intensity in north urban China in 2020 [1]. Copyright © 2023, Springer Nature Limited. (B) Historical CO_2 emissions from centralized heating at the national level [2]. Copyright © 2023, Elsevier. (C) Residential end-use CO_2 emissions in urban areas [3]. Copyright © 2023, Elsevier.

materials (PCMs), as visually depicted in Figure 2. PCMs serve as thermal energy storage (TES) mediums, capable of absorbing and releasing thermal/cold energy through alterations in their physical states. This property enables PCMs to effectively store solar energy during periods of abundant solar radiation and subsequently release heat as needed, thereby significantly mitigating building heating demands [4,5]. Furthermore, as elucidated in Figure 3, PCMs can be broadly categorized into three types based on their state transitions during the phase change process: liquid-gas PCMs, liquid-solid PCMs, and solid-solid PCMs. It is noteworthy that salt hydrate PCMs offer several advantages [6], including high thermal conductivity, versatile operating temperature ranges, cost-effectiveness, non-toxicity, and non-flammability, summarized in Table 1. Consequently, salt hydrate PCMs hold substantial promise for large-scale engineering applications.

PCMS-ENHANCED BUILDING ENERGY STORAGE SYSTEMS

Currently, substantial research has focused on three categories of energy storage systems leveraging PCMs in buildings, as depicted in Figure 4. These categories include PCMs-enhanced building facilities, PCMs-enhanced building envelopes, and PCMs-enhanced geostructures [4,5,7–11]. PCMs-enhanced building energy storage systems enable the storage of thermal or cold energy during off-peak periods, releasing it during peak demand times, effectively reducing overall energy demand within buildings [5,10]. However, it is crucial to note that PCMs must be tailored to meet precise temperature requirements during their applications. For facility systems, PCMs must exhibit a suitable phase change temperature. In thermal storage applications like domestic hot water, PCMs with a melting temperature (T_m) typically within 45–50°C enhance the coefficient of performance (COP) of heat pump systems [5,12]. This aligns with the maximum temperature achievable by conventional air-source heat pumps, approximately 55°C [13]. For cold storage,

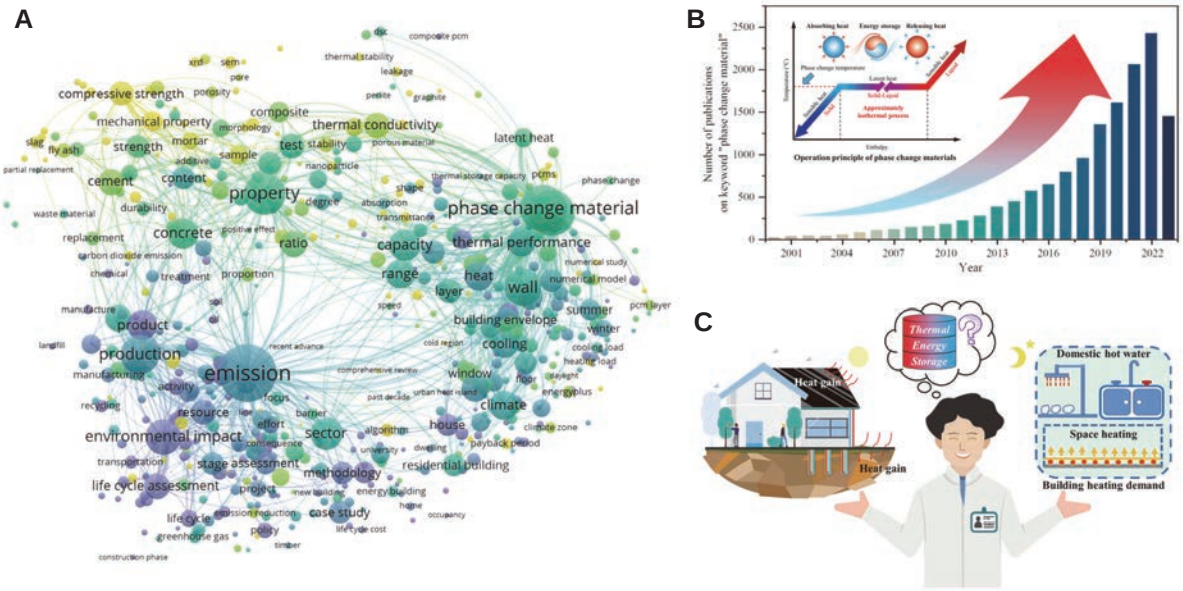

Figure 2 Investigation of PCM applications in buildings. (A) Cluster analysis graph depicting the keywords "reduce building energy consumption" and "material" using VOS viewer. (B) Number of publications on the keyword "phase change material" from 2000 to 2023 (data as of September 2023 from Web of Science). (C) Schematic diagram illustrating the relationship between heat gain and building heat demand.

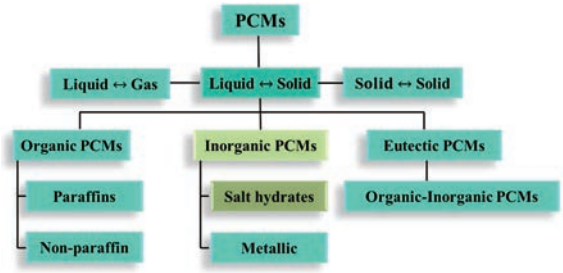

Figure 3 Classifications of PCMs.

Table 1 Comparison between organic PCMs and salt hydrate PCMs

Comparison	Organic PCMs	Salt hydrate PCMs
Advantages	Non-corrosive	High thermal conductivity
	Low supercooling degree	High volumetric latent heat storage
	Good chemical and thermal stability	Low price
Disadvantages	Low volumetric latent heat storage capacity	High supercooling degree
	Low thermal conductivity	Prone to phase separation
	High flammability and toxic combustion products	Corrosion to metals

PCMs should have a proper crystallization temperature, typically within 7–10°C, aligning with the lowest temperature achievable by conventional chiller cooling water, approximately 5°C [14].

For applications like heat storage in drying agricultural or food products, PCMs with phase change temperatures within 50–60°C are suitable. Conversely, for indoor temperature regulation, their phase change temperatures should align with thermal comfort, typically within 20–28°C [4,7,15,16]. When PCMs enhance

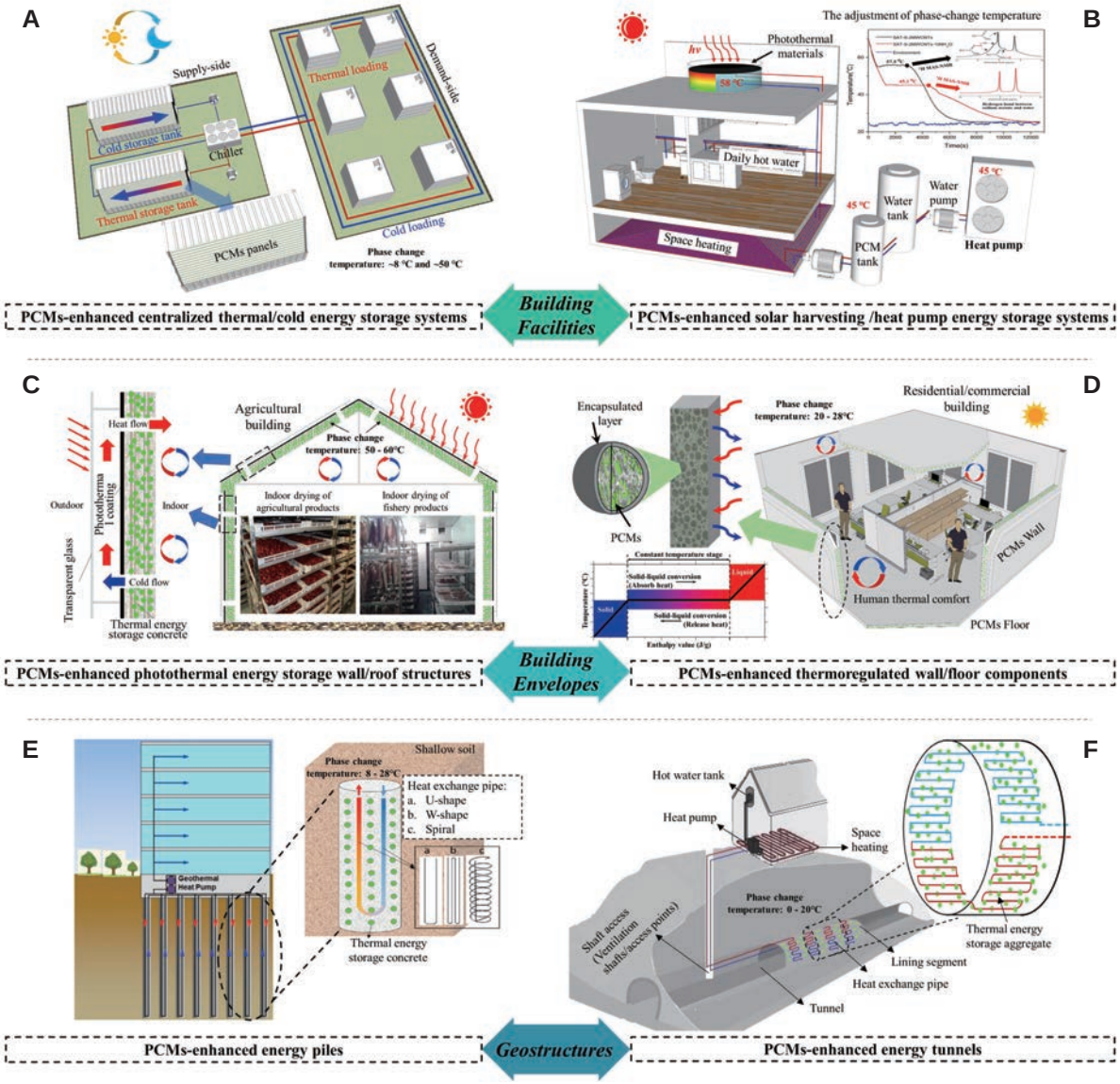

Figure 4 Schematic of various PCMs-enhanced energy storage systems in buildings. (A) PCMs-enhanced centralized thermal/cold storage systems. (B) PCMs-enhanced solar harvesting/heat pump energy storage systems. (C) PCMs-enhanced photothermal energy storage wall/roof structures. (D) PCMs-enhanced thermoregulated wall/floor components. (E) PCMs-enhanced energy piles and (F) PCMs-enhanced energy tunnels. Adapted with permission from refs. [4,5,7–11], Copyright © 2023, Elsevier, Copyright © 2022, Elsevier, Copyright © 2022, Elsevier, Copyright © 2022, Elsevier, Copyright © 2022, Elsevier, Copyright © 2018, Elsevier, Copyright © 2019, Elsevier.

the energy density of geostructures, their temperature characteristics become pivotal. Specifically, for shallow geothermal energy, PCMs should operate within the temperature range of 8–28°C, while for low ground temperature geothermal energy, the range should be within 0–20°C. This aligns with the operational requirements of cold/heat energy demand for the above-ground construction [9,17]. Therefore, it is evident that low-temperature salt hydrate PCMs play a vital role as latent heat storage materials in contemporary research. Table 2 presents a compilation of various types of salt hydrate PCMs that meet the temperature requirements of the building energy storage systems mentioned above.

Table 2 Types of low-temperature salt hydrate PCMs (below 120°C) [a] [18–20]

Salt hydrate PCMs	Melting temperature (°C)	Supercooling degree (°C)	Latent heat (J/g)	Thermal conductivity (W/(m K))	Analytical reagent grade (CNY/kg)	Other grades (CNY/kg)	Industrial grade (Corresponding salt, CNY/kg)	Chemical abstracts service number
$LiClO_3·3H_2O$	8	6	253.0	0.8	3083.8	3083.8 (99.9% metals basis)	–	13453-78-6
$ZnCl_2·3H_2O$	10	–	–	–	767.0 *	420.0 (chemically pure grade)	0.426	7646-85-7
$K_2HPO_4·6H_2O$	14	–	109.0	–	101.4 *	61.8 (purity 99%)	0.043	7778-77-0
$KF·4H_2O$	18.5	33	231.0	–	140.0 *	104.9 (purity 95%)	0.860	7789-23-3
$K_2HPO_4·4H_2O$	18.5	–	231.0	–	101.4 *	61.8 (purity 99%)	0.043	7778-77-0
$FeBr_3·6H_2O$	21	–	105.0	–	– *	3327.8 (purity 98%)	28.000	10031-26-2
$LiBO_2·8H_2O$	25.7	–	289.0	–	– *	4927.8 (purity ⩾ 99.9%)	1.600	13453-69-5
$Mn(NO_3)_2·6H_2O$	25.8	20	125.9	–	–	3003.8 (purity 98%)	–	17141-63-8
$CaCl_2·6H_2O$	29	30	190.8	0.5	48.0 *	32.0 (purity 96%)	0.009	10043-52-4
$LiNO_3·3H_2O$	30	40	296.0	–	1095.8 *	1355.8 (99.9% metals basis)	–	7790-69-4
$Na_2SO_4·10H_2O$	32	20	254.0	0.6	51.1	145.8 (guaranteed reagent grade)	0.350	7727-73-3
$Na_2CO_3·10H_2O$	32	–	246.5	0.5	63.2	68.0 (guaranteed reagent grade)	0.152	6132-02-1
$LiBr·2H_2O$	34	–	124.0	–	– *	1946.3 (purity ⩾ 99%)	1.520	7550-35-8
$CaBr_2·6H_2O$	34	60	115.5	–	– *	8580.0 (purity ⩾ 96%)	1.040	7789-41-5
$Na_2HPO_4·12H_2O$	35	20	280.0	0.5	156.5	196.7 (guaranteed reagent grade)	0.020	10039-32-4
$Zn(NO_3)_2·6H_2O$	36.4	–	147.0	0.5	257.4	1449.8 (99.99% metals basis)	–	10196-18-6
$FeCl_3·6H_2O$	37	–	223.0	–	144.0	103.5 (purity 98%)	–	10025-77-1
$Mn(NO_3)_2·4H_2O$	37.1	–	115.0	–	–	1423.8 (purity 98%)	–	20694-39-7
$CoSO_4·7H_2O$	40.7	–	170.0	–	297.6	1078.8 (99.99% metals basis)	0.375	10026-24-1
$KF·2H_2O$	42	–	162.0	–	561.2	721.8 (purity 98%)	–	13455-21-5

(*To be continued on the next page*)

(*Continued*)

Salt hydrate PCMs	Melting temperature (°C)	Supercooling degree (°C)	Latent heat (J/g)	Thermal conductivity (W/(m K))	Analytical reagent grade (CNY/kg)	Other grades (CNY/kg)	Industrial grade (Corresponding salt, CNY/kg)	Chemical abstracts service number
$Ca(NO_3)_2·4H_2O$	43	65	138.0	–	478.0	3805.8 (99.98% metals basis)	–	13477-34-4
$Fe(NO_3)_2·9H_2O$	47	–	155.0	–	187.2	1320.0 (99.9% metals basis)	0.125	7782-61-8
$K_2HPO_4·3H_2O$	48	–	99.0	–	156.5	1180.4 (99.99% metals basis)	0.019	16788-57-1
$Na_2S_2O_3·5H_2O$	48	65	209.0	0.4	–	41.7 (guaranteed reagent grade)	0.064	10102-17-7
$Na_2HPO_4·7H_2O$	48	–	170.0	–	318.8	284.0 (purity ⩾ 98%)	0.019	7782-85-6
$MgSO_4·7H_2O$	48.5	–	202.0	–	44.2	59.2 (guaranteed reagent grade)	0.345	10034-99-8
$Na(CH_3COO)·3H_2O$	58	90	270.3	0.9	46.0	50.0 (guaranteed reagent grade)	0.028	6131-90-4
$Cd(NO_3)_2·4H_2O$	59.5	–	–	–	169.6	2157.8 (99.99% metals basis)	–	10022-68-1
$FeSO_4·7H_2O$	64	–	200.0	–	68.1	1577.8 (99.95% metals basis)	0.028	7782-63-0
$Na_2P_2O_7·10H_2O$	70	70	184.0	–	94.0	–	0.035	13472-36-1
$Li(CH_3COO)·2H_2O$	70	–	150.0	–	734.5	873.6 (99.9% metals basis)	1.600	6108-17-4
$Al(NO_3)_2·9H_2O$	72	–	155.0	–	78.3	1143.2 (99.99% metals basis)	–	7784-27-2
$Ba(OH)_2·8H_2O$	78	–	265.7	0.7	176.9	136.5 (purity ⩾ 98%)	0.595	12230-71-6
$Al2(SO_4)_3·18H_2O$	88	27	–	–	73.2	94.8 (purity ⩾ 99%)	0.780	7784-31-8
$Mg(NO_3)_2·6H_2O$	89	70	162.8	0.6	–	–	–	13446-18-9
$KAl(SO_4)_2·12H_2O$	91	–	269.0	–	50.4	–	0.048	7784-24-9
$(NH_4)Al(SO_4)_2·12H_2O$	95	–	269.0	–	37.3	64.4 (chemically pure grade)	0.850	7784-26-1
$MgCl_2·6H_2O$	117	80	168.6	0.6	112.0	39.6 (purity = 98%)	0.390	7791-18-6

a: * denotes the anhydrous salt; the prices of analytical reagent grade and other grades of salt hydrate PCMs were sourced as of November 2023 from https://www.aladdin-e.com/ and http://www.macklin.cn/, while the prices of industrial-grade salt hydrate PCMs were obtained as of November 2023 from https://www.1688.com/.

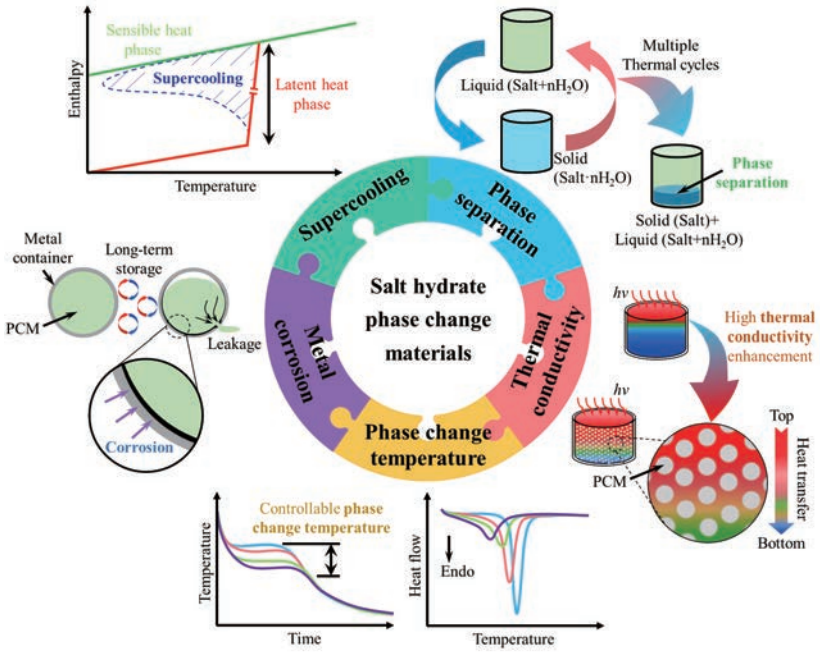

Figure 5 Challenges of utilizing salt hydrate PCMs in buildings.

CHALLENGES ASSOCIATED WITH THE APPLICATIONS OF SALT HYDRATE PCMS

While the utilization of salt hydrate PCMs in various building energy storage systems holds promise for reducing overall energy consumption, several challenges must be addressed before their practical engineering applications, as shown in Figure 5. The first significant challenge pertains to their poor nucleation characteristics, leading to substantial supercooling degree and impeding efficient energy storage charging. The second challenge revolves around phase separation, a consequence of the incongruent melting behavior of salt hydrates during the phase change process. As the number of energy storage cycles increases, solid salt gradually accumulates at the container's bottom and, due to gravitational forces, does not redissolve into water during the melting process. The third challenge lies in the inadequate thermal conductivity of PCMs (below 0.7 W/(m K)). While their thermal conductivity surpasses that of organic PCMs, achieving higher thermal conductivity remains desirable to enhance heat exchange efficiency further. The fourth challenge concerns the ability to control the phase change temperatures of salt hydrates, making them suitable for diverse energy storage systems. Lastly, salt hydrates are corrosive to metals, potentially leading to leakage in metal containers used for heat exchange enhancement and corrosion of metal fins employed for thermal conductivity enhancement.

REVIEW FRAMEWORK

Over the last few years, several review papers have been published to consolidate the periodic accomplishments in salt hydrate research. Wong-Pinto *et al*. [19] and Zahir *et al*. [21] delved into the supercooling

of salt hydrates, particularly in the context of optimization with nanomaterials and triggering techniques. Kumar *et al*. [22], Schmit *et al*. [23], Yu *et al*. [24], and Liu *et al*. [25] focused on topics such as thermal conductivity enhancements, phase transition enthalpies, and shape stabilization of salt hydrates. However, these existing reviews have omitted a critical analysis of salt hydrate modification methods and their underlying mechanisms. Consequently, this paper seeks to comprehensively review these mechanisms before and after the optimization of salt hydrates, drawing insights from existing literature across five key areas: supercooling, phase separation, thermal conductivity, phase change temperature, and metal corrosion, as illustrated in Figure 5.

SUPERCOOLING

Supercooling represents a metastable state of PCMs, wherein they remain in a liquid phase below the melting temperature without an instantaneous release of latent heat of fusion. The stability of supercooled solutions is often assessed using the hydrochemical potential as an indicator, with Eq. (1) illustrating this relationship:

$$\Delta\mu_{H_2O} = \mu c - \mu m = \mu s - \mu m = RT\ln\frac{a_s}{a_m}, \quad (1)$$

where a_m, a_s, and T denote the supercooled water activity, water activity of saturated solution, and storage temperature, respectively; $\Delta\mu_{H_2O}$ denotes the difference in water chemical potential (the supercooled solution is stable when $\Delta\mu_{H_2O} > 0$); μc, μm, and μs denote the chemical potential of hydrated salt crystals, the chemical potential of the supercooled solution, and the chemical potential of saturated hydrated salt solution, respectively.

Upon demand, the supercooled solution can be triggered to coagulate and crystallize, releasing the latent heat of melting and enabling long-term stable TES [26]. Take sodium acetate trihydrate (SAT) as an example, Dannemand *et al*. [27] and Johansen *et al*. [28] utilized stable supercooled solution to achieve trans-seasonal heat migration with low heat loss over a period of about two and five months, respectively. However, the metastable nature of supercooled solutions makes them susceptible to impurities and external disturbances, including the supercooling stabilizer [29], container design [30], and external environment [31]. Premature crystallization leads to ineffective energy consumption in the overall system [32], particularly in large-volume thermal storage systems [33]. In contrast, short-term flexible TES is more desirable for a broader range of applications.

The metastable state of PCMs is generally unsuitable for short-term flexible TES, impeding their rapid thermal storage/release in high-efficiency applications [21,34]. Researchers have quantified this phenomenon by characterizing the supercooling degree, which denotes the disparity between the T_m and the solidification temperature (T_s), as illustrated in Figure 6A. Over the past few decades, numerous strategies have been developed to minimize this undesirable supercooling effect. These strategies include the use of additives, external field control, and various other methods [35], with additives emerging as the prevailing and cost-effective approach in current research [36]. Effectively mitigating the supercooling tendencies of salt hydrates requires a comprehensive understanding of their nucleation mechanisms, as depicted in Figure 6B, showcasing various methods and summarizing current research progress in this area.

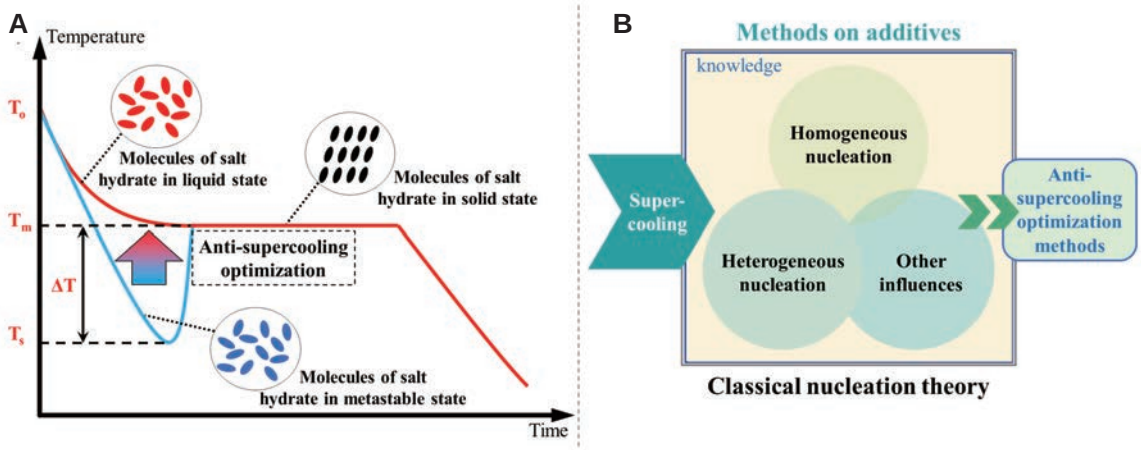

Figure 6 Schematic illustration of nucleation mechanisms of salt hydrate PCMs. (A) Schematic of temperature vs. time curve measured by *T*-history method and (B) nucleation methods to promote the crystallization of salt hydrate PCMs.

Anti-supercooling mechanism based on the classical nucleation theory

The classical nucleation theory (CNT) stands as the most widely accepted theoretical model for the investigation of crystal nucleation. It encompasses two primary nucleation processes: homogeneous and heterogeneous nucleation [37]. Therefore, this section primarily delves into homogeneous and heterogeneous nucleation through the lens of Gibbs free energy to elucidate the mechanism behind countering supercooling in salt hydrate PCMs. The Gibbs free energy is a pivotal factor in determining the direction of thermodynamic processes. If the Gibbs free energy is negative under constant temperature and pressure, an isothermal or isostatic reaction is considered spontaneous; otherwise, it is non-spontaneous. When the Gibbs free energy is zero, the reaction is in equilibrium. Hence, the reduction of Gibbs free energy is typically regarded as the driving force behind the transition from liquid to solid phases.

Homogeneous nucleation

Homogeneous nucleation is a spontaneous and random process where the probability of a crystal nucleus forming from a uniform single-phase solute is uniformly distributed. According to the Gibbs free energy theory, the formation of crystals hinges on the difference between the volume free energy (ΔG_V) and surface energy (ΔG_S) of the emerging nucleus, as illustrated in Figure 7A. Equation (2) delineates the change in free energy during the transition from a liquid to a solid state. In this process, ΔG_V serves as the driving force, while ΔG_S represents the barrier force. Figure 7B illustrates how Δg can be calculated as outlined in Eqs. (3)–(5), and Figure 7C presents the schematic diagram of the crystal growth process.

The variation mentioned is written as [38]

$$\Delta G = \Delta G_V + \Delta G_S = V\Delta g + A\sigma = -4\pi r^3 \Delta g / 3 + 4\pi r^2 \sigma, \quad (2)$$

where Δg denotes the difference in free energy per unit volume between the liquid and solid states when thermodynamic phase nucleation occurs, and σ indicates the surface tension of the interface between the nucleus and its surroundings. The components of the above equations are as follows:

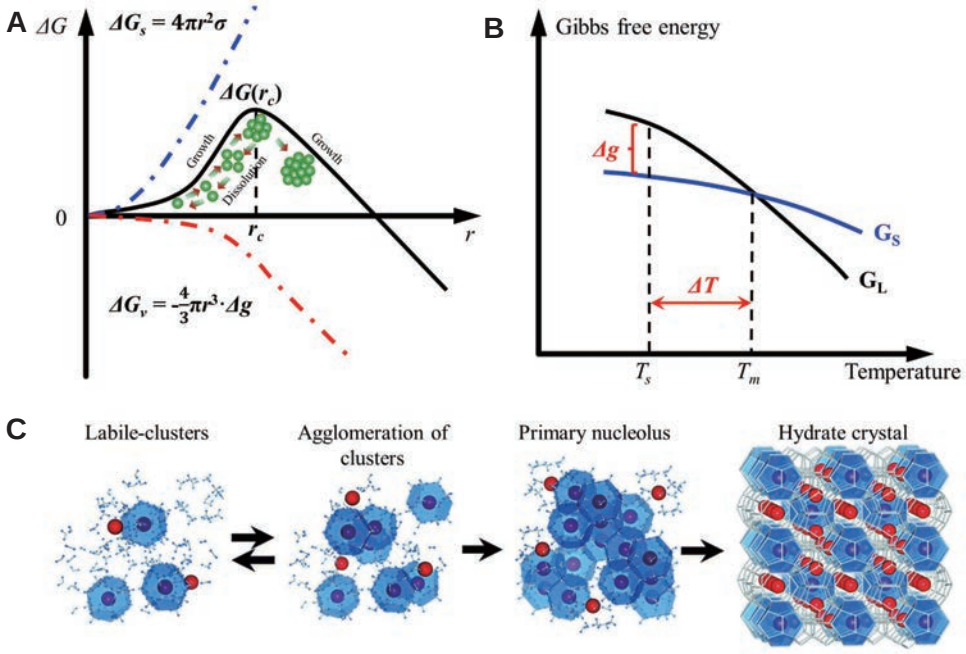

Figure 7 Variation of Gibbs free energy for a transition from the liquid state to solid state. (A) Relationship between the nucleation radius and Gibbs free energy. (B) Relationship between the temperature and Gibbs free energy. (C) Labile-cluster model of hydrate nucleation [37]. Copyright © 2020, Royal Society of Chemistry. Note: ΔG denotes the Gibbs free energy; $\Delta G(r_c)$ denotes the Gibbs free energy corresponding to the critical radius; Δg and ΔT denotes the difference in free energy per unit volume and supercooling degree of PCMs, respectively.

$$\Delta g = \Delta G_{ss} - \Delta G_{ls} = \Delta H_{ss} + \Delta T\,\Delta S_{ss} - \Delta H_{ls} + \Delta T\,\Delta S_{ls} = \Delta H - \Delta T\,\Delta S, \tag{3}$$

$$\Delta S = \Delta H / T_m, \tag{4}$$

$$\Delta g = \Delta H\,\Delta T / T_m, \tag{5}$$

where ΔG_{ss} and ΔG_{ls} denote the Gibbs free energies of the solid and liquid states of the PCM, respectively; ΔH_{ss} and ΔH_{ls} denote the enthalpies of the solid and liquid states of the PCM, respectively; ΔS_{ss} and ΔS_{ls} denote the entropies of the solid and liquid states of the PCM, respectively.

When ΔG_S reaches its maximum value, the critical radius (r_C) can be determined by taking its derivative, such that $\Delta G = 0$, expressed as

$$r_C = 2\sigma / \Delta g = 2T_m\sigma / \Delta H\,\Delta T. \tag{6}$$

This implies that only nuclei larger than a critical nucleus size are thermodynamically stable and capable of growing to a detectable size, while smaller nuclei dissolve. In the initial stages of crystal nucleation, PCM molecules diffuse to the forming nucleus and adhere to its surface. Consequently, these minute crystals continue to expand through this mechanism, gradually reaching a size where they can sustain rapid crystal growth [37,39,40].

From Eq. (6), it is evident that, under constant pressure, crystals can only form after the salt hydrate PCMs have undergone the supercooling stage. Considering Eqs. (2)–(6), it can be deduced that the minimum Gibbs free energy for the formation of crystals must satisfy the following Eq. (7) [41]:

$$\Delta G(r_C) = 16\pi T_m\sigma^3 / 3\Delta H^2\Delta T^2. \tag{7}$$

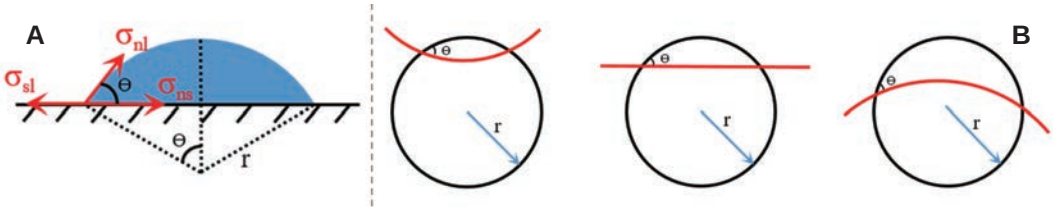

Figure 8 Schematic of the contact angle between the crystal nucleus, liquid medium, and substrate surfaces for different structures. (A) The nucleus growing on the surface of a flat substrate [42]. Copyright © 2022, Elsevier. (B) The nucleus growing on the substrate surface under different structures for identical nucleation radii and contact angles.

Heterogeneous nucleation

Unlike homogeneous nucleation, which occurs spontaneously and randomly within a uniform solution, heterogeneous nucleation takes place on foreign particles or sites. These sites could include the container wall, impure particles, or unmelted crystal grains present in the liquid salt hydrates [34]. Besides, the crystal particles of nucleating agents or nuclei are formed by the liquid salt hydrates. From Figure 8A, it can be deduced that the Gibbs free energy of heterogeneous nucleation process can be expressed as the following equations [8–17]:

The process mentioned is written as [4,42]

$$\Delta G_S = A_{nl} \cdot \sigma_{nl} + A_{ns} \cdot \sigma_{ns} - A_{sl} \cdot \sigma_{sl}, \tag{8}$$

$$\sigma_{sl} = \sigma_{nl}\cos\theta + \sigma_{ns}, \tag{9}$$

$$A_{ns} = A_{sl} = \pi r^2 \sin^2\theta, \tag{10}$$

$$A_{nl} = 2\pi r^2(1-\cos\theta), \tag{11}$$

$$\Delta G_S = 2\pi r^2(1-\cos\theta)\sigma_{nl} - \pi r^2 \sin^2\theta\cos\theta\sigma_{nl}, \tag{12}$$

$$V = \pi r^3(2-3\cos\theta+\cos^3\theta/4), \tag{13}$$

$$\Delta G = -\Delta G_V + \Delta G_S = -V\Delta g + A\sigma = \left(-4\pi r^3\Delta g/3 + 4\pi r^2\sigma_{nl}\right)\cdot f(\theta), \tag{14}$$

$$f(\theta) = 2-3\cos\theta+\cos^3\theta/4, \tag{15}$$

$$r_C = 2\sigma/\Delta g = 2T_m\sigma/\Delta H\Delta T, \tag{16}$$

$$\Delta G_{heterogeneous} = \Delta G_{homogeneous} f(\theta) = \frac{16\pi T_m\sigma^3}{3\Delta H^2\Delta T^2} f(\theta), \quad 0 < f(\theta) < 1, \tag{17}$$

where θ denotes the contact angle between the crystal nucleus and substrate surface; A_{nl}, A_{ns}, and A_{sl} denote the surface areas between the crystal-nucleation and liquid phases, crystal-nucleation and substrate surfaces, and substrate surface and liquid phase, respectively; σ_{nl}, σ_{ns}, and σ_{sl} denote the surface energy between the crystal-nucleation and liquid phases, crystal-nucleation and substrate surfaces, and substrate surface and liquid phase, respectively.

The critical radius of heterogeneous nucleation matches that of homogeneous nucleation, as determined from Eqs. (16) and (17). However, the key distinction lies in the Gibbs free energy, which is lower for heterogeneous nucleation compared with homogeneous nucleation, and this difference depends on the contact angle. Consequently, it can be inferred that the nucleation barrier for heterogeneous nucleation is significantly lower than that for homogeneous nucleation.

In addition to the supercooling degree and contact angle, the substrate surface morphology has also been identified as a factor influencing crystal crystallization, as illustrated in Figure 8B. When the critical radius and contact angle are the same, the volume of the nucleus, which must reach the critical radius, varies based on different interface morphologies. The concave surface exhibits the highest nucleation efficiency as it can most readily reach the critical radius of the crystal nucleus and requires a smaller embryo volume. Following this, the plane curvature efficiency is moderate, while the efficiency of the convex surface is the lowest. Consequently, the degree of supercooling varies depending on the surface morphology of the same type of nucleating agent.

Other influences on supercooling

In the CNT theory, the degree of supercooling in salt hydrates is primarily influenced by the contact angle and the morphology of the substrate. However, there are additional factors that can impact supercooling. Both Kubota *et al*. [43] and Lopez *et al*. [44] observed a size effect on the degree of supercooling during phase transitions in a KNO_3 aqueous solution and VO_2 nanoparticles, respectively. They found that smaller samples exhibited a higher degree of supercooling compared with larger ones. This phenomenon is attributed to the reduction in the total number of nucleation sites as the sample size decreases, leading to a lower likelihood of nucleation. According to the CNT theory, Reference [45] presented that the probability of successful nucleation at a specific temperature $P(T)$ can be described by Eq. (18).

$$P(T)\mathrm{d}T = 1 - \exp\left[-C\left|\Delta T\,\Delta H / T_{\mathrm{m}}\right|^{y} \cdot V\right], \tag{18}$$

where $P(T)$ denotes the likelihood of successful nucleation at specific temperatures; C, y and V denote a proportionality constant, an exponent, and the test sample volume, respectively.

A higher cooling rate has been found to increase the degree of supercooling [46]. In the experiment conducted by Taylor *et al*. [47] using commercial hydrated calcium chloride salts, it was observed that the degree of supercooling rises with an increase in the cooling rate, as illustrated in Figure 9A. A similar phenomenon was reported by Solomon *et al*. [48], who attributed the change in PCM solidification temperature to the cooling rate (Figure 9B). Mollova *et al*. [45], in experiments with PCMs under varying cooling rates (ranging from 0.01 to 500 K), noted that higher cooling rates led to increased supercooling. This can be explained by either the growth of crystals, which depends on the crystal growth rate and takes time, or a significant reduction in the nucleation rate at lower temperatures. Oike *et al*. [49] further expanded on this by proposing that both the cooling rate and the volume of specimens significantly impact the degree of supercooling. They speculated that the sample volume to cooling rate ratio is closely related to the likelihood of nucleation at a specific temperature and developed a prediction model described in Eq. (19).

$$P(T)\mathrm{d}T = i_{\mathrm{v}}^{\mathrm{hetero}}(T) \cdot (V/r)\mathrm{d}T \cdot \exp\left[-(V/r)\int_{T}^{T_{\mathrm{m}}} i_{\mathrm{v}}^{\mathrm{hetero}}(T')\mathrm{d}T'\right], \tag{19}$$

where $i_{\mathrm{v}}^{\mathrm{hetero}}(T)$ and r represent the heterogeneous nucleation rate density and cooling rate, respectively.

Anti-supercooling optimization methods

Various methods have been explored to mitigate supercooling in salt hydrate PCMs, with a focus on

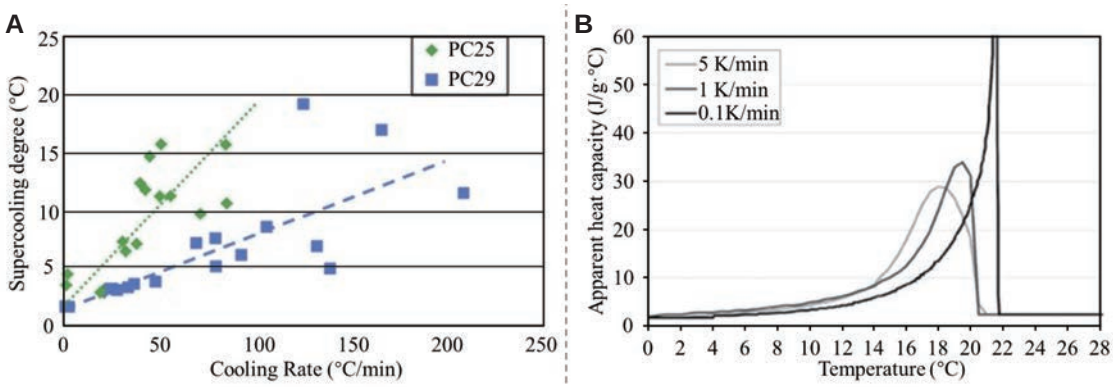

Figure 9 Effect of cooling rate. (A) Supercooling degree as a function of cooling rate (the dashed lines give the linear trends of the data) [47]. Copyright © 2016, Elsevier. (B) DSC analysis of commercial PCM for different cooling rates [48]. Copyright © 2013, Elsevier.

Table 3 Crystal structures of salt hydrate PCMs and their potential nucleating agents

Salt hydrate PCMs		*a* (Å)	*b* (Å)	*c* (Å)	*β* (angle)	T_m (°C)
Salt hydrate PCMs	$CaCl_2·6H_2O$	7.860	–	3.87	–	30.0
Potential nucleating additive	$SrCl_2·6H_2O$	7.940	–	4.108	–	61.4
Salt hydrate PCMs	$Na_2SO_4·10H_2O$	1.116	1	1.238	107°45′	32.3
Potential nucleating additive	$Na_2B_4O_7·10H_2O$	1.114	1	1.114	107°33′	75.0
Salt hydrate PCMs	$MgCl_2·6H_2O$	9.90	7.15	6.10	94°00′	117
Potential nucleating additive	$MgBr_2·6H_2O$	10.25	7.40	6.30	93°30′	165

promoting heterogeneous nucleation. Both internal and external factors impact crystallization, including the supercooling degree, contact angle, nucleation rate, and crystal growth rate. External factors like the sample volume and cooling rate also play a role in influencing supercooling. These factors contribute to different supercooling degrees for the same types of salt hydrates, even when uniform types and dosages of nucleating agents are used. Consequently, this section reviews various techniques aimed at reducing the supercooling of salt hydrate PCMs, with an emphasis on heterogeneous nucleation.

Addition of other types of salt hydrates

The lattice-matching method, proposed by Telkes [50] and Lane [51], offers a systematic approach to selecting suitable nucleating agents. According to this method, when the lattice constants of the salt hydrate crystal and the nucleating agent differ by less than 15%, and the nucleating agent's melting temperature exceeds that of the salt hydrate crystal, the nucleating agents can effectively reduce the supercooling degree of salt hydrates. The effectiveness of salt hydrate nucleating agents largely depends on their affinity for the crystals. High affinity results in a low contact angle and vice versa. Through crystallographic databases, it has been found that certain nucleating agents, such as borax ($Na_2B_4O_7·10H_2O$) and $SrCl_2·6H_2O$, are highly effective for specific salt hydrates like Glauber's salt ($Na_2SO_4·10H_2O$) and $CaCl_2·6H_2O$, respectively, as presented in Table 3. Telkes [50] discovered that incorporating 1.4% $Na_2B_4O_7·10H_2O$ prevented the supercooling degree of a supersaturated Glauber salt solution from exceeding 2°C. Similarly, Li *et al*. [52] achieved a supercooling degree as low as 2.8°C by adding 4 wt.% $SrCl_2·6H_2O$.

Table 4 Summary of the supercooling characteristics of nanomaterial-modified salt hydrate PCMs

Salt hydrate PCMs	Nucleating agents (wt.%)	Specimen size (g)	Supercooling degree (°C)		Latent heat capacity (J/g)	Reference
			Original	Modified		
$CH_3COONa·3H_2O$	Nano Cu particle (0.5)	Not mentioned	>20	0.5	242.4	[57]
$CH_3COONa·3H_2O$	Chitin nanowhiskers (1.0)	5	>20	0.87	241	[58]
$CH_3COONa·3H_2O$	Nano aluminum nitride particle (5)	Not mentioned	17	0.1	238.5	[59]
$CH_3COONa·3H_2O$ and KCl (92:8)	Nano-α-Al_2O_3 (1)	50	7.3	0.1	241.2	[56]
$Na_2SO_4·10H_2O$ and $Na_2HPO_4·12H_2O$ (20:80)	Nano-α-Al_2O_3 (4.5)	Not mentioned	7.8	1.6	256.9	[60]
$KAl(SO_4)_2·12H_2O$ and $Na_2SO_4·10H_2O$ (65:35)	Nano-carbon particle (1.0)	Not mentioned	2.9	1.8	132.2	[61]
$CaCl_2·6H_2O$	Nano Cs_xWO_3 (0.75)	20	7.81	0.61	138.6	[62]

In the quest to reduce supercooling in salt hydrates, the lattice-matching principle is not the sole criterion for selecting nucleating agents. Researchers have discovered that certain non-isomorphous and non-isotypic salt additives can effectively suppress supercooling in salt hydrates. Employing an empirical approach, Zhang *et al*. [53] observed that pure $Na_2S_2O_3·5H_2O$ failed to crystallize at a phase change temperature of ~48°C, even when the test specimen was cooled to an ambient temperature of ~20°C. However, the addition of 0.08 wt.% sodium pyrophosphate ($Na_4P_2O_7$) induced solidification at 46.8°C. Similarly, Mao *et al*. [54,55] determined that $Na_2HPO_4·12H_2O$ was the most effective nucleating agent for $CH_3COONa·3H_2O$ when compared with $Na_2HPO_4·12H_2O$, $Na_2B_4O_7·10H_2O$, $Na_2CO_3·10H_2O$, $Na_3PO_4·12H_2O$, and $Na_2SiO_3·9H_2O$. Through this method, they achieved a supercooling degree of ~2°C with the addition of 5 wt.% $Na_2HPO_4·12H_2O$. Although non-isomorphous and non-isotypic salt hydrates can effectively suppress supercooling, the mechanisms behind their nucleation-promoting effects remain unclear.

Moreover, salt crystals themselves have been shown to aid in reducing supercooling in salt hydrates. Li *et al*. [56] demonstrated that the inclusion of potassium chloride (KCl) could decrease the supercooling degree of SAT while also lowering the phase change temperature. In their study, when SAT was mixed with 2, 4, and 6 wt.% KCl, the supercooling degree decreased to 9.2, 3.5, and 3.1°C, and the phase change temperatures were lowered to 54, 53, and 52°C, respectively, from the original 58°C. Equation (16) suggests that reducing the melting temperature is a means to inhibit supercooling in salt hydrate PCMs, as it decreases the total Gibbs free energy of nucleation, facilitating crystal nucleation. Therefore, anti-supercooling can also be achieved by adding substances that lower the phase change temperatures of salt hydrates.

Addition of nanomaterials

Table 4 provides an overview of the supercooling characteristics of nanomaterial-modified salt hydrates. It is evident that the supercooling degree can be dramatically reduced, sometimes even to within 0.1°C, through the addition of suitable nanomaterials. However, the mechanism underlying this reduction has not been definitively established, and only a few possible mechanisms are currently proposed.

Li *et al*. [56] suggested that nano-Al_2O_3 can serve as numerous nucleation sites, acting as scaffolds for the attachment and growth of $CH_3COONa·3H_2O$ crystals. This process is illustrated in Figure 10. The surface of nano-Al_2O_3 carries a negative charge due to hydroxyl groups, which strongly interact with Na^+ ions. This

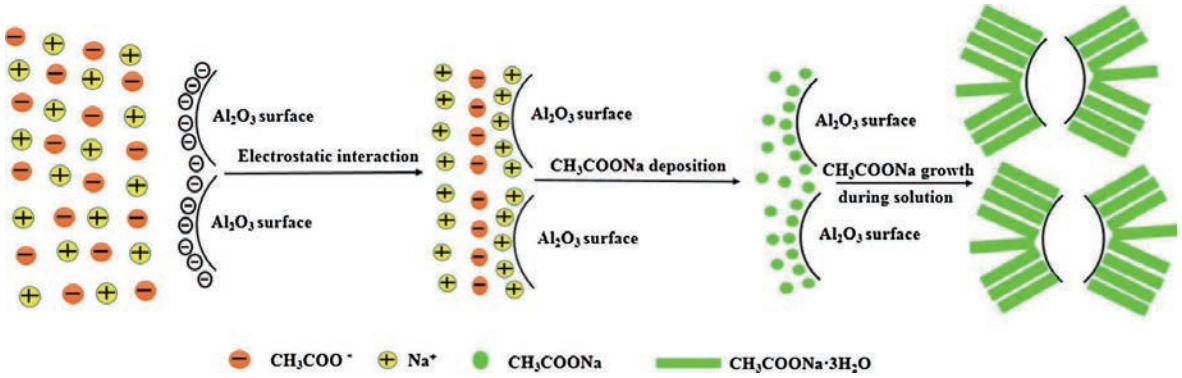

Figure 10 Schematic of the nucleation mechanism of $CH_3COONa·3H_2O$ on the surface of nano-Al_2O_3 [56]. Copyright © 2016, Elsevier.

interaction increases the number of $CH_3COO–$ and H_2O molecules adsorbed onto the surface of nano-Al_2O_3. However, adding excessive nanomaterials can lead to aggregation due to their extremely high specific surface areas. When nanoscale Al_2O_3 aggregates into non-nanoscale particles, its effectiveness diminishes as a nucleating agent for suppressing supercooling.

Moreover, Zhang *et al*. [63] agreed that nanomaterials are more effective nucleating agents than micro-sized materials because their diameters closely match the critical radius of nucleation crystals. Only a small fraction of crystal formation is required to initiate nucleation. This nucleation mechanism aligns with the one depicted in Figure 8B. Furthermore, Cui *et al* [4,42] observed that the supercooling degree of SAT could be reduced by 1.58°C from 32°C with the addition of 10 wt.% expanded perlite (EP), but significantly further reduced to 1.4°C with the addition of 2 wt.% nano silica (NS). They noted that the contact angles between the liquid PCMs and NS were only 28.0°, as shown in Figure 11, promoting heterogeneous nucleation and further decreasing the degree of supercooling. This is because the free energy of the nucleation barrier in PCMs is reduced by approximately 95%. However, experimental observations of salt hydrate nucleation facilitated by nanomaterials remain limited, and this possibility is mostly theoretical at this stage.

Other optimization methods on anti-supercooling

Hydrophilic porous media have proven effective in reducing the supercooling of hydrated salts. The hydrophilic surfaces of porous media facilitate the adsorption of water molecules and salt ions due to capillary action and surface tension. This promotes the heterogeneous nucleation of hydrated salts, as depicted in Figure 12. Yang *et al*. [64] discovered that when $CaCl_2·6H_2O$, $CH_3COONa·3H_2O$, and $Na_2SO_4·10H_2O$ were absorbed into diatomite, the supercooling degrees of salt hydrate PCMs were reduced by at least 10, 40, and 10°C, respectively. Similarly, Wang *et al*. [65] employed three-dimensional (3D) graphene as a carrier to absorb $Na_2SO_4·10H_2O$, resulting in a decrease of approximately 5°C in the supercooling degree.

Moreover, other methods such as external field control (e.g., magnetic field, ultrasound, mechanical vibration [66], electric field, and microwave) and other techniques (e.g., wire interference and surface tension) can also be used to suppress supercooling. Although Zhao *et al*. [35] discussed several methods and techniques in a review that piqued researchers' interest, achieving anti-supercooling solutions for salt hydrate PCMs through controllable external fields remains in the experimental stage and can be expensive.

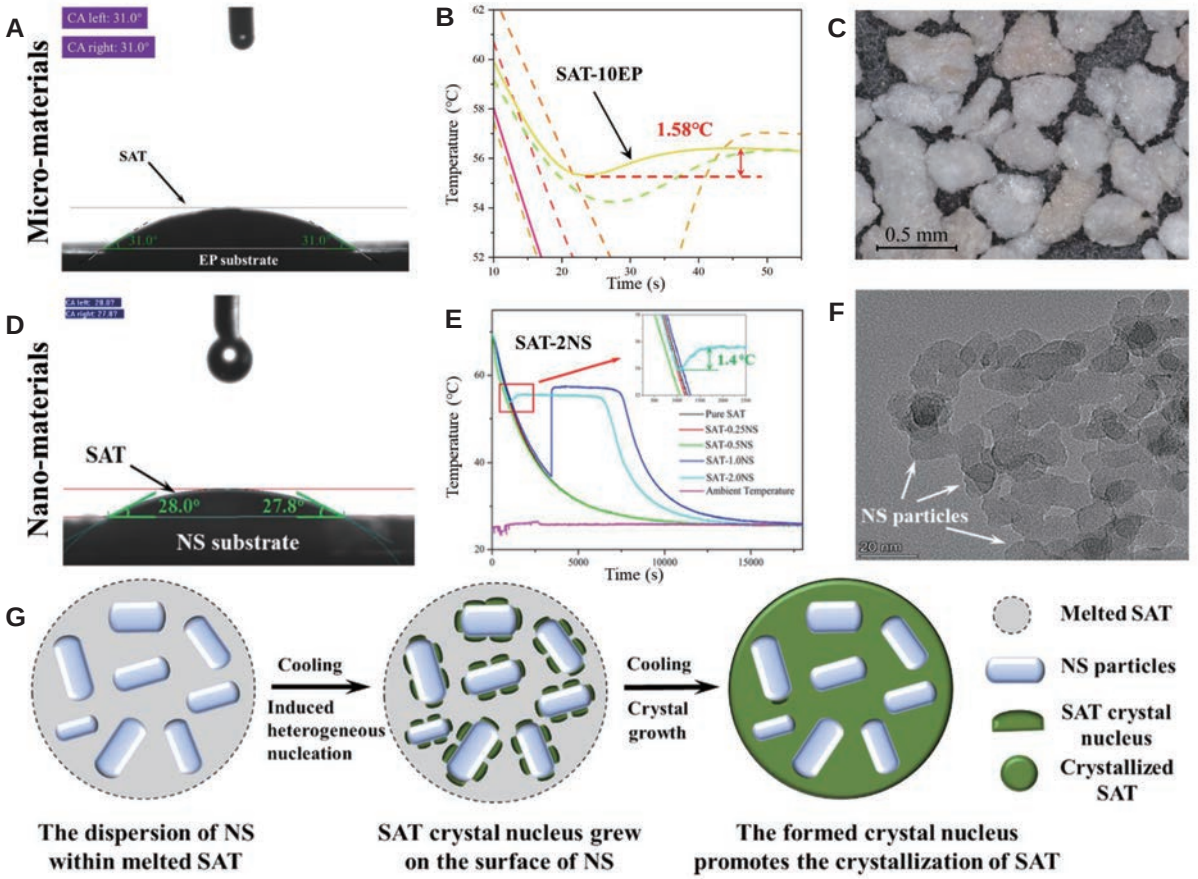

Figure 11 Comparison of the anti-supercooling effect of modified $CH_3COONa{\cdot}3H_2O$ composites using micro-materials and nano-materials. (A) Contact angle between EP and liquid SAT. (B) Supercooling degree of SAT-10EP. (C) The morphology of EP particles. (D) Contact angle between NS and liquid SAT. (E) Supercooling degree of SAT-2NS. (F) Morphology of NS particles. (G) Possible nucleation mechanism of NS on the crystallization of SAT. Adapted with permission from references [4,42], Copyright © 2023, Elsevier, Copyright © 2022, Elsevier.

PHASE SEPARATION

Salt hydrate PCMs exhibit incongruent melting during the endothermic process, leading to phase separation during multiple thermal cycles, as shown in Figure 13. The phase separation, characterized by some of the anhydrous salt settling to the bottom of the container due to gravity, can result in a progressive degradation of the heat-storage capacity of the salt hydrates and a reduction in their service life. Additionally, nucleating agent particles in salt hydrate liquids or solids can deposit and aggregate, exacerbating the issue of supercooling. Therefore, addressing phase separation in salt hydrate PCMs is a pressing concern. This section reviews several empirical measures proposed in the literature to tackle this problem. However, these methods still have some shortcomings and remain a focus of ongoing research.

Thickening

Thickening involves adding thickening materials to the salt hydrate liquid to increase its viscosity. This helps

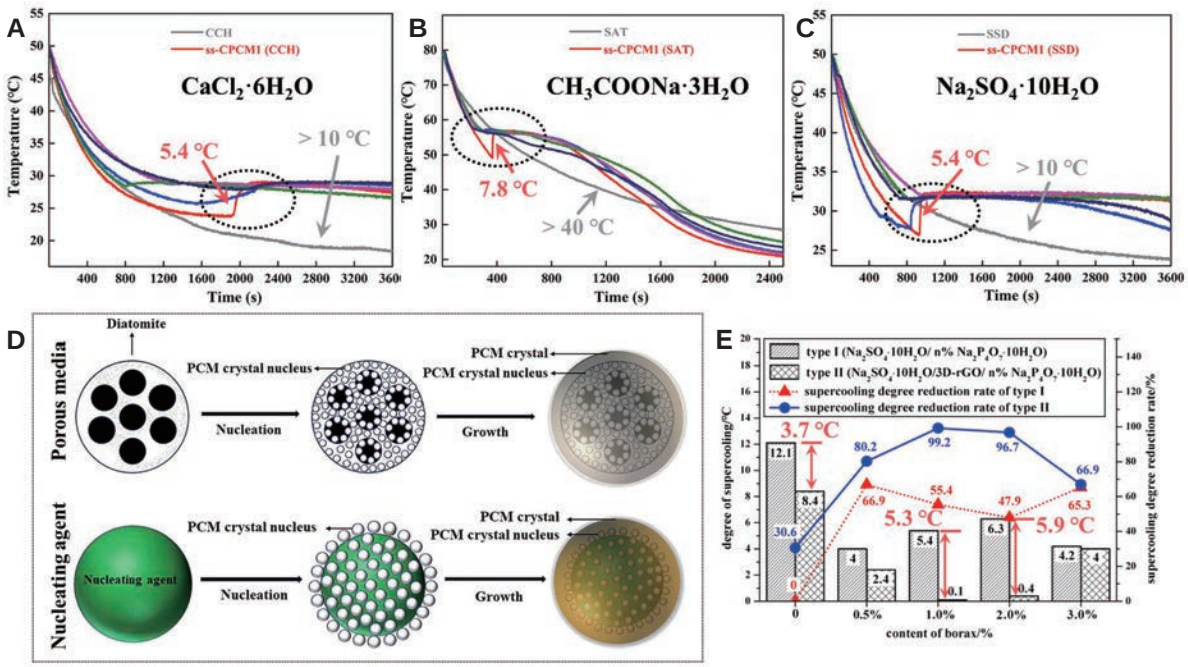

Figure 12 Effect of porous media on the anti-supercooling of salt hydrate PCMs. (A) Step-cooling curves of diatomite porous media containing $CaCl_2·6H_2O$. (B) Step-cooling curves of diatomite porous media containing $CH_3COONa·3H_2O$. (C) Step-cooling curves of diatomite porous media containing $Na_2SO_4·10H_2O$. (D) Comparison of nucleation mechanisms by porous media and nucleating agent. (E) Influence of 3D-rGO porous media on the supercooling degree and the corresponding supercooling degree reduction rate of $Na_2SO_4·10H_2O$. Adapted with permission from references [64,65], Copyright © 2019,Wiley, Copyright © 2018, Wiley.

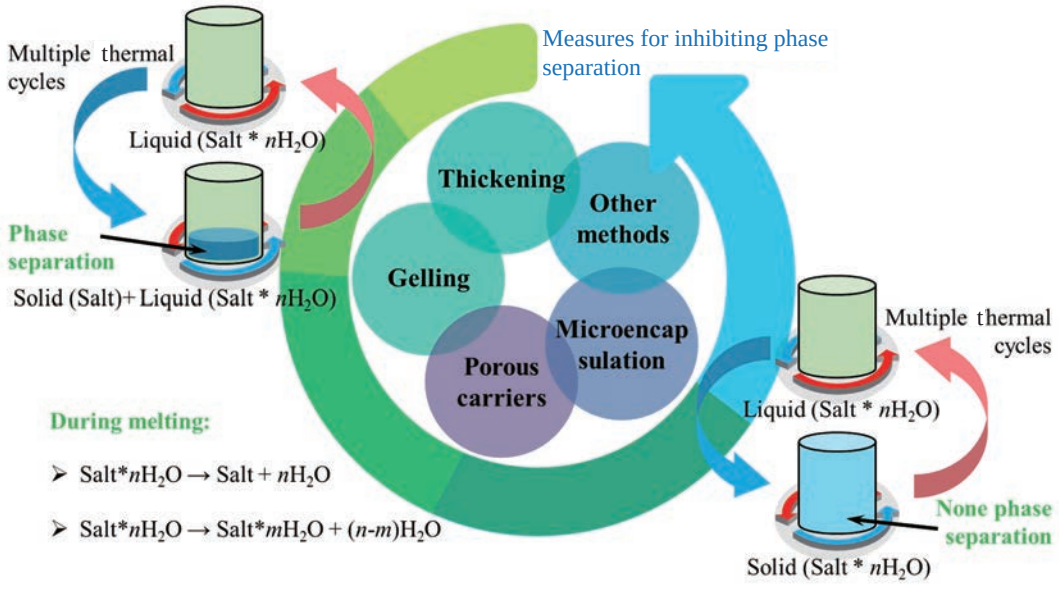

Figure 13 Methodology for inhibition of phase separation of salt hydrate PCMs.

Table 5 Summary of thickeners for various salt hydrate PCMs

Salt hydrate PCMs	Thickeners	Latent heat capacity (J/g)		Reference
		Original	After cycling	
$Na_2SO_4·10H_2O$ (3 wt.% $Na_2B_4O_7·10H_2O$)	Attapulgite clay (9 wt.%)	~238 (without thickener) ~203	~63 (20–40 cycles) ~105 (200 cycles)	[67]
$CaCl_2·6H_2O$ (0.5 wt.% flake graphite)	Super-absorbent polymer (25 wt.%)	198.4 (without thickener) 158.4	– –	[68]
$CaCl_2·6H_2O/ChCl_2$ (2 wt.% $SrCl_2·6H_2O$)	Silica fumes (2 wt.%)	127.2 (without thickener) 123.0	– 122.69 (100 cycles)	[69]
$CH_3COONa·3H_2O$ (1 wt.% $Na_2HPO_4·7H_2O$)	Cellulose-based thickeners (30 wt.%)	~243 (without thickener) ~165	– –	[70]
$CH_3COONa·3H_2O$ (0.5% Nano-Cu and 0.25% sodium dodecyl sulfonate)	Carboxymethyl cellulose (3 wt.%)	242.4 (without thickener) 234.5	– 231.4 (50 cycles)	[57]
$CH_3COONa·3H_2O$ (2 wt.% multi-wall carbon nanotubes)	Xanthan gum (1 wt.%)	257.7 (without thickener) 250.2	– 241.3 (500 cycles)	[5]

reduce the phase-separation rate, improving the uniformity of salt hydrates in solution and enhancing their long-term stability during multiple hydration/dehydration thermal cycles. The mechanisms of thickeners can be summarized as follows: First, the hydrophilic chains of thickeners associate with surrounding water molecules through hydrogen bonds, forming a gel-like structure that increases the system's viscosity. Second, thickeners swell after absorbing water to form a flocculent substance, which combines with water to create a colloid. However, it is crucial to select the appropriate thickener, as excessive amounts can make sample preparation difficult and lead to the formation of air bubbles, resulting in poor PCM performance.

Table 5 lists different thickeners for different salt hydrate PCMs. Marks [67] found that 9% attapulgite clay could eliminate the segregation of $Na_2SO_4·10H_2O$ and stated that the addition of thickeners effectively delays the decline in the storage capacity of salt hydrate PCM systems. Bao *et al*. [68] discovered that adding 25 wt.% super-absorbent polymers eliminated the segregation of $CaCl_2·6H_2O$. Meanwhile, Shahbaz *et al*. [69] concluded that 2 wt.% silica fumes could also achieve the same effect, and the salt hydrate PCM composite exhibited good thermal stability after 100 cycles. More recently, Yang *et al*. [5] eliminated segregation by thickening $CH_3COONa·3H_2O$ with xanthan gum, and the material showed improved thermal stability after 500 cycles. However, Kumar *et al*. [22] noted that the effectiveness of thickening depends on the chemical compatibility between the thickener and salt hydrate. Therefore, developing or discovering more effective thickeners is still a research priority.

Additionally, Efimova *et al*. [71] found that while some thickeners are effective in the short term, they may lose their effectiveness when subjected to long-term thermal cycling. As depicted in Figure 14, even with the addition of thickeners like SiO_2 and methylcellulose, some inorganic salts may still precipitate during long-term use. To the best of our knowledge, existing literature does not provide evidence that a specific thickener's performance can guarantee the stability of salt hydrate PCMs after enduring more than 5000 thermal cycles.

Consequently, ensuring the long-term stability and reliability of thickeners remains a significant research challenge, as it is crucial for the practical application of salt hydrate PCMs in engineering. Moreover, various measures can be explored to restore the unstable state of salt hydrate PCMs after prolonged operation, drawing inspiration from the self-healing mechanisms observed in materials like concrete [72].

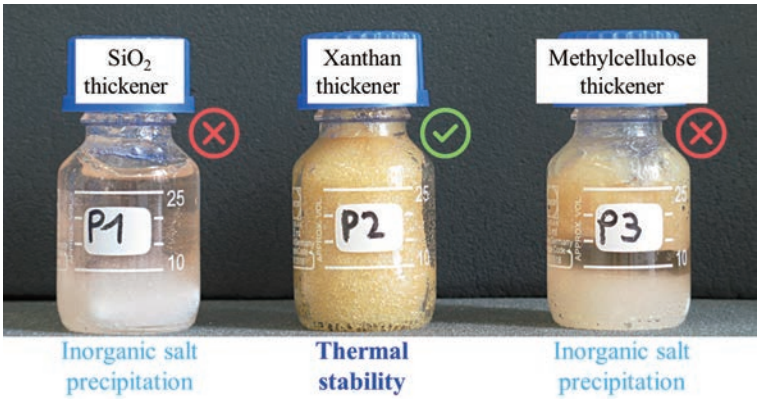

Figure 14 Ternary salt hydrate specimens [$Zn(NO_3)_2{\cdot}6H_2O/Mn(NO_3)_2{\cdot}4H_2O/KNO_3$] with thickening agent SiO_2, xanthan, or methylcellulose after 480 freezing/melting cycles [71]. Copyright © 2015, Elsevier.

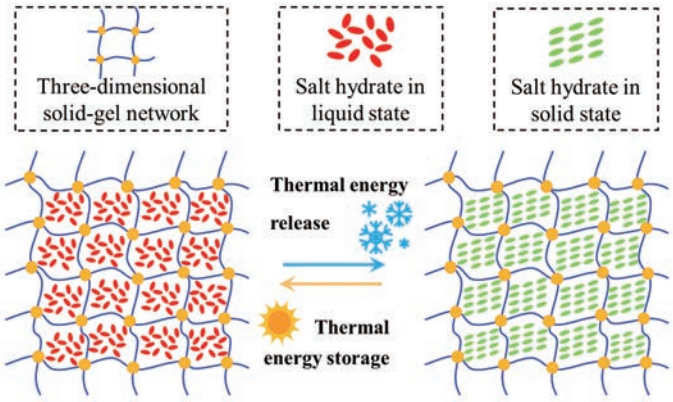

Figure 15 Schematic of the gelling mechanism of salt hydrate PCMs.

Gelling

Gelling involves the addition of a crosslinking agent to thickened salt hydrates, creating a 3D solid-gel structure, as shown in Figure 15. The PCMs loaded into this network structure can store and release thermal energy during the phase change process, making it an efficient and reliable solution for various applications [4].

However, research on gelled salt hydrates is relatively limited, and only a few studies have reported on this approach. In 2007, Lan *et al*. [73] applied gelation technology to confine salt hydrates within a restricted space. They used polymers such as sodium acrylate, sodium alginate, *N*,*N*-methylene bisacrylamide, and crosslinking agents like $K_2S_2O_8$ and Na_2SO_3. This resulted in the growth of most $Na_2HPO_4{\cdot}12H_2O$ crystals being less than 0.1 mm, and the latent heat of their salt hydrate PCMs remained constant after 50 thermal cycles. Similarly, Liu *et al*. [74,75] used carbon nanotubes and graphene oxide as crosslinking agents for acrylate-sodium-based polymers, achieving excellent thermal and chemical stability after 500 thermal cycles. In addition, Karimineghlani *et al*. [76] discovered that certain thickeners can directly form gels with salt hydrates without requiring crosslinking agents. For instance, polyvinyl alcohol (PVA) as a thickener can be

mixed with lithium nitrate trihydrate to create a solid gel due to the crosslinking induced by Li^+ ions.

Compared with thickeners, gelled salt hydrates do not flow and possess a consistency similar to jelly-like pastes, often exhibiting mechanical properties to some extent. Recently, using a similar strategy, Cui *et al*. [3] introduced an innovative TES aggregate based on salt hydrate PCMs. This approach resulted in excellent thermal stability and mechanical strength, leading to desirable thermal and mechanical properties for TES concrete. In summary, gelling is a promising technology for inhibiting phase separation in salt hydrate PCMs, as it can create a more stable matrix for these materials. This advancement represents a significant step toward facilitating the practical application of salt hydrate PCMs.

Porous carriers

Porous materials are commonly employed as supporting materials to contain salt hydrates, mitigating phase separation. This approach capitalizes on the capillary force, Van der Waals force, surface tension, and hydrogen bonds between the salt hydrates and the porous matrixes [77]. Porous materials serve as effective carriers for salt hydrates, as each pore in the porous structure functions as a miniature encapsulator, providing a heterogeneous surface where salt hydrate droplets can be captured. Notably, porous aggregates such as EP [4,78,79], expanded vermiculite [80–82], and diatomite [83,84] have been found to be chemically compatible with salt hydrate PCMs, as shown in Figure 16, making them suitable carriers. Notably, to ensure the long-term stability and reliability of salt hydrate PCMs when used in practical engineering applications, coating systems can be employed. These systems effectively encapsulate the porous carriers and their contents, preventing leakage and ensuring the sustained performance of salt hydrate PCMs over multiple thermal cycles. This combination of porous carriers and protective coatings represents a promising solution for various TES applications.

The analysis from Table 6 reveals that the loading capacity of salt hydrates into porous aggregates typically exceeds 50 wt.%, with the specific capacity influenced by the type of salt hydrates due to differences in viscosity. Moreover, the fact that salt hydrate PCMs maintain a high latent heat even after multiple thermal cycles underscores the excellent thermal stability provided by porous aggregates. However, it is crucial to emphasize that porous carriers containing salt hydrates still require additional coating measures before they can be incorporated into cement-based materials. Despite the use of vacuum pressure to immerse salt hydrate PCMs into the porous carrier, there remains a risk of leakage after multiple cycles, which could potentially affect the corrosion of steel reinforcement within structural elements. Essentially, while salt hydrates are contained within the pore structure, they are not fully isolated from the external environment. This allows for an exchange between the internal ions of the salt hydrate and the free water present in the cement-based materials. Therefore, it is necessary to provide external protection to porous carriers containing salt hydrates, and this can be further understood through previous research on coating system strategies for PCMs [85].

Microencapsulation

Microencapsulation is a valuable technique for addressing the phase separation issues associated with salt hydrate PCMs. This technology involves encapsulating salt hydrates within protective shells, preventing their contact with the external environment and effectively inhibiting phase separation, as depicted in Figure

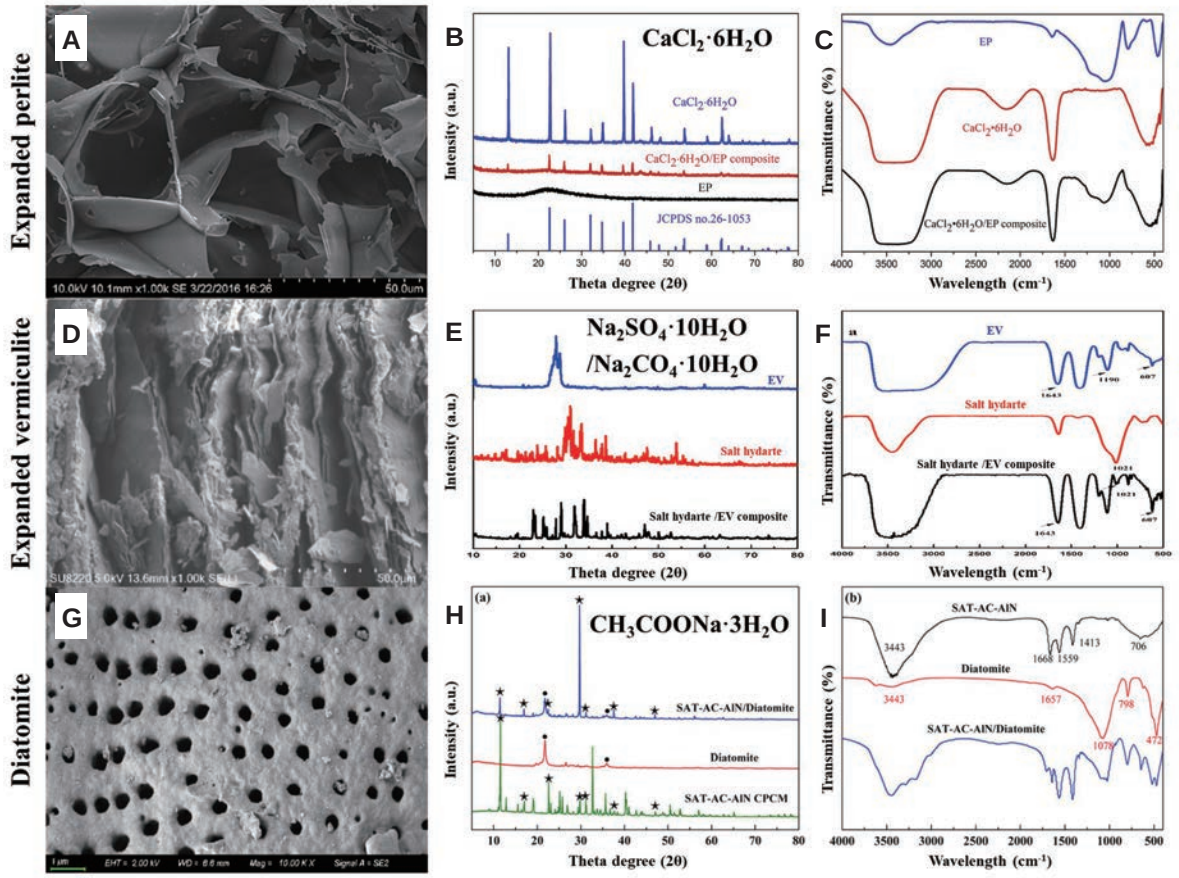

Figure 16 Morphologies of different porous carriers and the chemical compatibility between salt hydrate PCMs and porous carriers. (A) SEM image of EP. (B) XRD pattern of EP containing $CaCl_2·6H_2O$. (C) Fourier transform infrared spectroscopy (FT-IR) of EP containing $CaCl_2·6H_2O$. (D) SEM image of expanded vermiculite. (E) XRD pattern of expanded vermiculite containing $Na_2SO_4·10H_2O$ and $Na_2CO_4·10H_2O$. (F) FT-IR spectrum of expanded vermiculite containing $Na_2SO_4·10H_2O$ and $Na_2CO_4·10H_2O$. (G) SEM image of diatomite. (H) XRD pattern of diatomite containing $CH_3COONa·3H_2O$. (I) FT-IR spectrum of diatomite containing $CH_3COONa·3H_2O$. Adapted with permission from references [78,81,84], Copyright © 2017, Elsevier, Copyright © 2019, Elsevier, Copyright © 2022, Elsevier.

Table 6 Summary of porous carriers for various salt hydrate PCMs [a]

Type of PCMs	Porous aggregate	Latent heat capacity (J/g)		Note	Reference
		Original	After cycling		
$CaCl_2·6H_2O/SrCl_2·6H_2O$ (98:2)	Expanded perlite (55% loading capacity)	87.44	76.46 (1000 cycles)	−5 to 50°C	[78]
$Na_2CO_4·10H_2O/Na_2HPO_4·12H_2O$ (5:5)	Expanded perlite (70% loading capacity)	151.73	91.99 (1000 cycles)	−20 to 60°C	[79]
$Na_2SO_4·10H_2O/Na_2CO_4·10H_2O$ (5:5)	Expanded vermiculite (60% loading capacity)	110.3	100.1 (100 cycles)	−10 to 50°C	[81]
$CH_3COONa·3H_2O$/ $Na_2B_4O_7·10H_2O$ (100:2)	Expanded vermiculite (86% loading capacity)	238.8	233.8 (150 cycles)	Unclarified	[82]
$Na_2HPO_4·12H_2O/Na_2CO_4·10H_2O$ (58:42)	Diatomite (58% loading capacity)	106.3	100.3 (300 cycles)	1.10 to 50°C	[83]
$CH_3COONa·3H_2O$	Diatomite (66% loading capacity)	162.5	159.6 (100 cycles)	20 to 65°C	[84]

a: Loading capacity denotes the ratio between the latent heat of raw salt hydrate PCMs and the latent heat of porous carrriers containing PCMs.

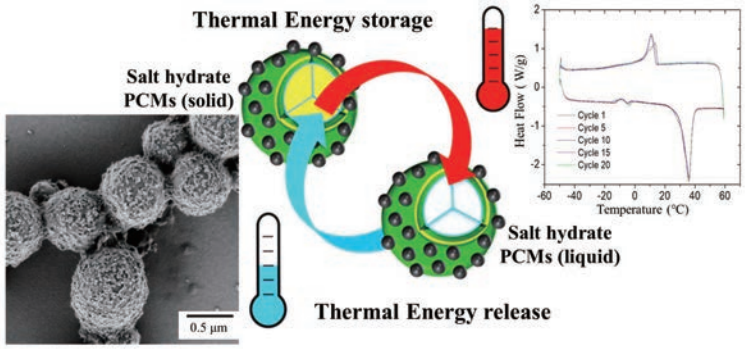

Figure 17 Microencapsulation technology for salt hydrate PCMs [86]. Copyright © 2020, American Chemical Society.

Table 7 Overview of microencapsulation technologies for various salt hydrate PCMs [a]

Type of PCMs	Encapsulation technique	Latent heat capacity (J/g)		Note	Reference
		Before cycling	After cycling		
$Na_2SO_4 \cdot 10H_2O$	Interfacial polymerization in nanoparticle-stabilized inverse emulsions (91.5% encapsulation capacity)	~60	~60 (20 cycles)	−50 to 90°C	[86]
$Na_2SO_4 \cdot 10H_2O$	Emulsion polymerization (59.3% encapsulation capacity)	125.6	100.9 (100 cycles)	−50 to 50°C	[88]
$Na_2HPO_4 \cdot 12H_2O$	Interfacial polymerization combined with sol-gel process (75.3% encapsulation capacity)	177.0	176.2 (30 cycles)	−30 to 55°C	[87]
$Na_2SO_4 \cdot 10H_2O$	Water-in-oil (W/O) emulsions (47.07% encapsulation capacity)	90.74	78.47 (100 cycles)	5 to 45°C	[89]
$Na_2S_2O_3 \cdot 5H_2O$	Sol-gel method (71.09% encapsulation capacity)	149.82	123.99 (200 cycles)	Unclarified	[90]

a: Encapsulation capacity denotes the ratio between the latent heat of raw salt hydrate PCMs and the latent heat of microencapsulation PCMs.

17. Various microencapsulation methods have been developed for salt hydrate PCMs, including improved interfacial polymerization [86,87], emulsion polymerization [88], water-in-oil (W/O) emulsions [89], and the sol-gel method [90].

Table 7 summarizes the research on microencapsulation for salt hydrate PCMs, and provides an overview of research on microencapsulation for salt hydrate PCMs. These studies have demonstrated the successful encapsulation of different salt hydrates using various materials and encapsulation techniques. For instance, tetraethoxysilane was used to synthesize SiO_2 shells for encapsulating $Na_2SO_4 \cdot 10H_2O$ [87,88], and methylmethacrylate and ethyl acrylate were employed to encapsulate $Na_2HPO_4 \cdot 7H_2O$ [91]. Microencapsulation technology effectively prevents phase segregation by isolating salt hydrates into individual microparticles. However, it is worth noting that microencapsulated salt hydrate PCMs may exhibit lower thermal stability compared with non-encapsulated counterparts, as observed in latent heat capacity after cycling (as discussed in Sections of Thickening and Porous carriers). Organic materials often make up a significant portion of the encapsulation materials, which can limit the improvement of heat transfer in PCMs. Future research in this area may focus on enhancing the mechanical strength of microencapsulated salt hydrate PCMs to better suit engineering applications, especially in scenarios involving complex thermal-mechanical conditions, such as structural function integrated energy storage concrete (Figure 4).

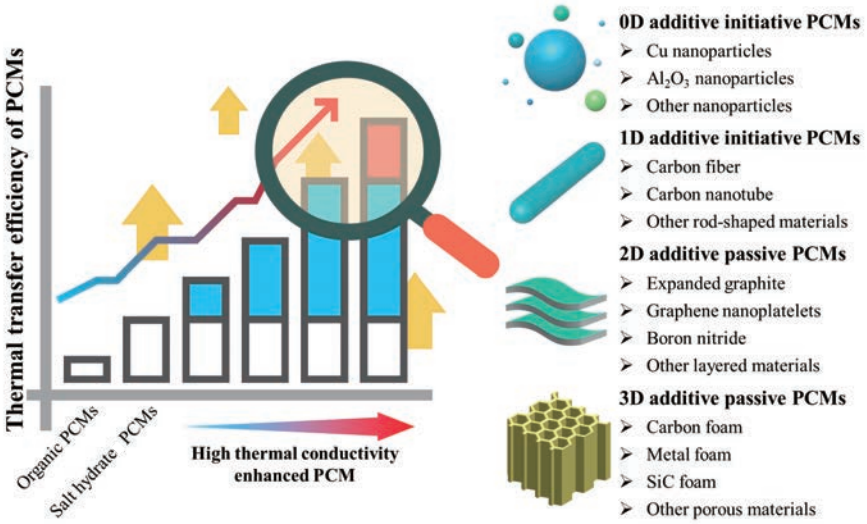

Figure 18 Methodology of thermal conductivity enhancement for salt hydrate PCMs.

Other optimization methods for phase separation

From an application perspective, phase separation, caused by inconsistent melting, can be mitigated by adding excess water to dilute salt hydrates, which is a straightforward and practical method [92]. This approach ensures a uniform distribution of all nearby PCM components to some extent and helps dissolve additional anhydrous salts deposited in the system, maintaining a saturated salt solution. However, a drawback of this method is a reduction in overall energy storage density due to dilution [93]. Additionally, the problems of supercooling and lower thermal conductivity resulting from extra water addition can be addressed using the techniques discussed in Sections of SUPERCOOLING and THERMAL CONDUCTIVITY.

Eutectic compositions are another technique employed to prevent phase separation and improve the thermal cycle stability of salt hydrate PCMs. This approach leads to a more stable structure through the rearrangement of hydrogen bonds [94]. For instance, a study by Zheng *et al*. [95] investigated PCMs with a mass ratio of 9:1 ($Na_2HPO_4 \cdot 12H_2O$ and $Na_2SO_4 \cdot 10H_2O$) to achieve improved thermal cycle stability.

THERMAL CONDUCTIVITY

Enhancing the thermal conductivity of PCMs is critical in improving their performance for TES applications. The existing literature provides various techniques for strengthening thermal transfer efficiency, ranging from macroscopic methods like fins to microscopic ones involving nanoparticles [22]. One way to assess thermal conductivity enhancement is by measuring the thermal conductivity of solid or liquid salt hydrate PCMs. High thermal conductivity can be achieved in PCMs by introducing various additives with different dimensional properties (0D, 1D, 2D, and 3D), as illustrated in Figure 18. These additives typically have significantly higher thermal conductivity than salt hydrate PCMs, which usually have thermal conductivities

Table 8 Summary of additives used to enhance thermal conductivity in salt hydrate PCMs [96–106]

Dimension	Additives		Thermal conductivity (W/(m K))
0D	Carbon	Graphite powder	500.0
	Metal	Cu nanoparticle	400.0
		Au nanoparticle	318.0
		Ni nanoparticle	90.3
		Ag nanoparticle	429.0
		Co_3O_4 nanoparticle	31.0
		Mg particles	156.0
	Ceramic	AlN powder	320.0
		Al_2O_3 nanoparticle	80.0
		SiC powder	150.0
1D	Carbon	Carbon fiber	900.0
		Carbon nanotube	4000.0
		Rod-shaped graphene	5300.0
	Metal	Ag nanowires	429.0
		CuO nanorod	32.9
	Ceramic	SiC nanowire	40.0
2D	Carbon	Expanded graphite	200.0
		Graphene nanoplatelet	3000.0
	Ceramic	hBN	3000.0
3D	Carbon	Graphite foam	200.0
		Diamond foam	10.7
	Metal	Al honeycomb	52.0
		Al foam	167.0
		Cu foam	401.0
		Ni foam	91.4
	Ceramic	SiC foam	170.0

in the range of 0.5 to 1.5 W/(m K) [22,96], as shown in Table 8.

Mechanism for thermal conduction enhancement

Heat transfer generally occurs through conduction, convection, or radiation, as illustrated in Figure 19A. Thermal conduction is the primary mode of heat transfer in solid materials, described by Eq. (20), which is derived from Fourier's law.

$$q = -K\nabla T, \tag{20}$$

where q, K, and ∇T represent the heat flow rate through a unit area per unit time, thermal conductivity, and the local temperature gradient, respectively.

The thermal conductivity of PCMs is influenced by various factors. Among them, phonon scattering is a critical factor that limits the thermal conductivity of PCMs. Phonons, which are quantized lattice vibrations, are responsible for heat transfer within materials. The thermal conductivity carried by phonons can be described using the Debye equation (Eq. (21) [107–109]) and Eq. (22), as depicted in Figure 19B.

$$K = \frac{1}{3}\int C_v(\omega)\cdot v(\omega)\cdot l(\omega)\mathrm{d}\omega, \tag{21}$$

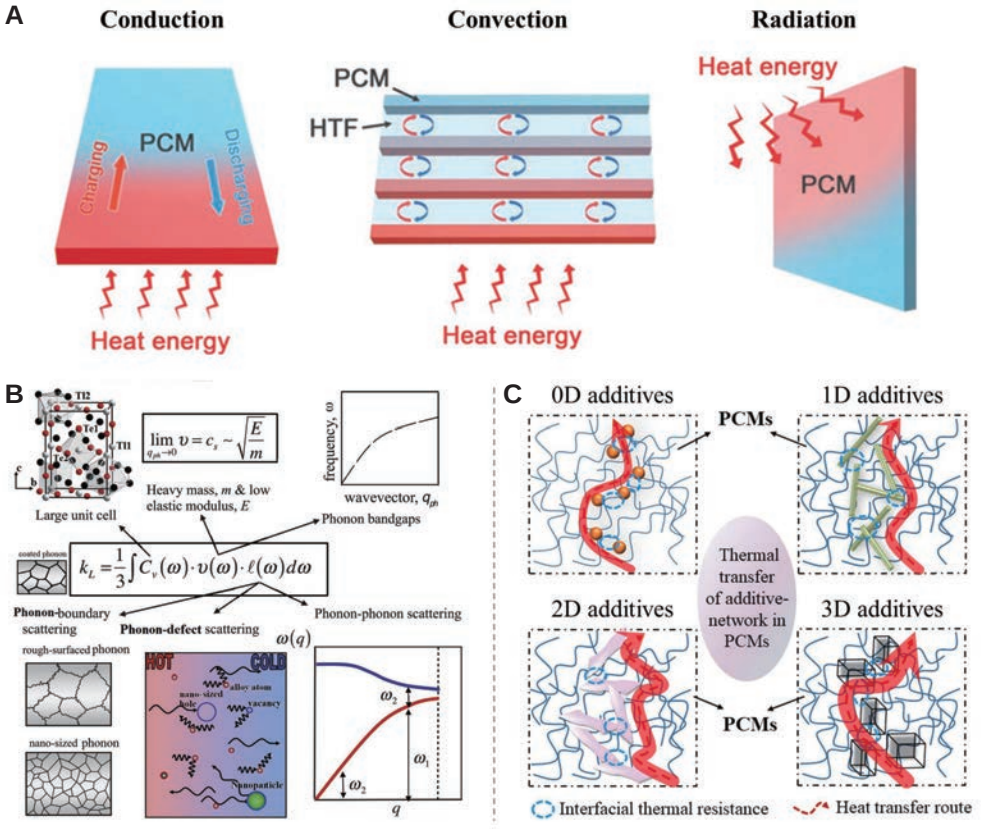

Figure 19 Mechanism of thermal conduction and enhancement in PCMs. (A) Schematic illustration of three basic heat transfer modes [110]. Copyright © 2019, Wiley. (B) Phonon thermal conductivity and related components [98]. Copyright © 2020, Elsevier. (C) Schematic illustration of heat transfer mechanism of PCMs enhanced by additives (modified by Reference [105]). Copyright © 2021, Elsevier.

$$v = \partial\omega(k) / \partial k, \tag{22}$$

where C_v, v, and l denote the specific heat capacity per volume, phonon group velocity, and mean free path of phonons in a material, respectively; ω and k denote the lattice vibration frequency and wavevector, respectively. The low phonon velocity and short mean free path contribute to the relatively low thermal conductivity of PCMs to some extent [105]. To enhance the thermal conductivity of PCMs, it is effective to incorporate additives with high thermal conductivity and thermal transfer efficiency. This strategy creates pathways or networks for heat transfer within the PCMs, as illustrated in Figure 19C.

Enhancing the thermal conductivity of salt hydrate PCMs

As depicted in Table 9, Cui *et al*. [57] conducted a study demonstrating that the incorporation of 0.5 wt.% nano copper (a 0D additive) into $CH_3COONa{\cdot}3H_2O$ resulted in a notable improvement in thermal conductivity, achieving an increase of 25.1%. In another study by Xiao *et al*. [111], copper foam (considered a 3D additive) was explored as a potential thermal conductivity enhancer. They found copper foam to be advantageous due to its ability to establish a continuous 3D structure that facilitates phonon propagation [112]. Consequently, when $CH_3COONa{\cdot}3H_2O$ was combined with copper foam, the thermal conductivity exhibited a remarkable increase of 176.3%.

Table 9 Comparison of thermal conductivity of salt hydrate PCMs before and after optimization with high-thermal-conductivity additives

Dimension of additives	Additives	Type of PCMs	Thermal conductivity (W/(m K))		Reference
			Before optimization	After optimization	
0D	Cu nanoparticle (0.5 wt.%)	$CH_3COONa·3H_2O$	0.921	1.155	[57]
	Carbon nanoparticle (1 wt.%)	$KAl(SO_4)_2·12H_2O$	0.546	0.910	[61]
	Graphite powder (2 wt.%)	$CH_3COONa·3H_2O$	0.630	0.850	[113]
	α-Al_2O_3 nanoparticle (4.5 wt.%)	$Na_2SO_4·10H_2O$	0.789	1.272	[60]
	γ-Al_2O_3 nanoparticle (2.0 wt.%)	$CaCl_2·6H_2O$	0.341	1.373	[114]
	AlN powder (9 wt.%)	$CH_3COONa·3H_2O$	0.562	0.680	[112]
	Modified AlN powder (16 wt.%)	$Na_2HPO_4·12H_2O$	0.500	1.400	[115]
	α-Fe_2O_3 nanoparticle (0.8 wt.%)	$CH_3COONa·3H_2O$	0.868	1.063	[116]
1D	Carbon nanotube (3 wt.%)	$CH_3COONa·3H_2O$	0.527	0.789	[5]
	Carbon fiber (8 wt.%)	$Na_2HPO_4·12H_2O$	0.500	1.910	[115]
	SiC nanowire (5 wt.%)	$Na_2SO_4·10H_2O$	0.781	1.016	[117]
2D	Hp-graphene nanoplatelet (5 wt.%)	$CH_3COONa·3H_2O$	0.650	1.930	[118]
	Graphene nanoplatelet (2.5 wt.%)	$Ba(OH)_2·8H_2O$	0.618	2.077	[119]
	hBN (5 wt.%)	$CH_3COONa·3H_2O$	0.700	1.200	[58]
	Expanded graphite (12 wt.%)	$CH_3COONa·3H_2O$	–	6.400	[120]
	Modified expanded graphite (26 wt.%)	$Ba(OH)_2·8H_2O$	–	3.580	[121]
	Graphite flake (5 wt.%)	$CH_3COONa·3H_2O$	0.590	1.100	[113]
3D	Cu foam (98% porosity)	$CH_3COONa·3H_2O$	0.760	2.100	[111]
	SiC foam (85% porosity)	$CH_3COONa·3H_2O$	0.64	1.540	[42]
	Cu foam (92.4% porosity)	$CH_3COONa·3H_2O$	0.590	6.800	[122]

Nevertheless, the inclusion of copper, a metal-based material, in salt hydrates comes with a significant risk of corrosion. Hence, researchers have focused on carbon-based and ceramic-based materials, which offer the dual advantages of high thermal conductivity and chemical inertness as thermal conductivity enhancers. These materials come in various dimensional forms. Among the 2D additives, such as graphene nanoplatelets [5], expanded graphite [120], and graphite flakes [113], expanded graphite displayed the optimal effects among them, as highlighted in Table 9. When 12 wt.% expanded graphite was introduced, the thermal conductivity saw a remarkable improvement to 6.4 W/(m K), constituting a 1225% increase. However, it is essential to note that expanded graphite is hydrophobic and does not adsorb salt hydrates in the same manner as organic PCMs. Consequently, the large particle size of expanded graphite limits the volumetric heat storage capacity. On the other hand, for ceramic-based materials, Cui *et al*. [42] recently developed an innovative SAT composite using SiC foam (a 3D additive) as the thermal conductivity enhancer. They also revealed the enhancement mechanism of 3D additives on the thermal conductivity of salt hydrate PCMs through microthermal infrared imaging, as depicted in Figure 20.

Moreover, rather than relying solely on individual additives, researchers have discovered that the thermal conductivity of salt hydrate PCMs can be further enhanced by combining additives of different dimensions, harnessing synergistic effects. A notable example is the collaborative effort by Yang *et al*. [5], who employed carbon nanotubes (1D additive) along with carbon fiber (1D additive), expanded graphite (2D additive), and graphene nanoplates (2D additive) to boost the thermal conductivity and photothermal charging efficiency of $CH_3COONa·3H_2O$, as illustrated in Figure 21. In their research, the thermal conductivity of salt hydrate

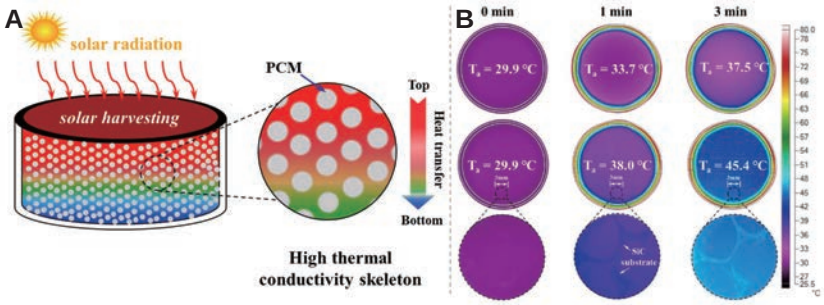

Figure 20 Enhancing the thermal conductivity of salt hydrate PCMs using three-dimensional additive. (A) Schematic of the enhancement mechanism and (B) thermal infrared imaging of the corresponding heat transfer process.

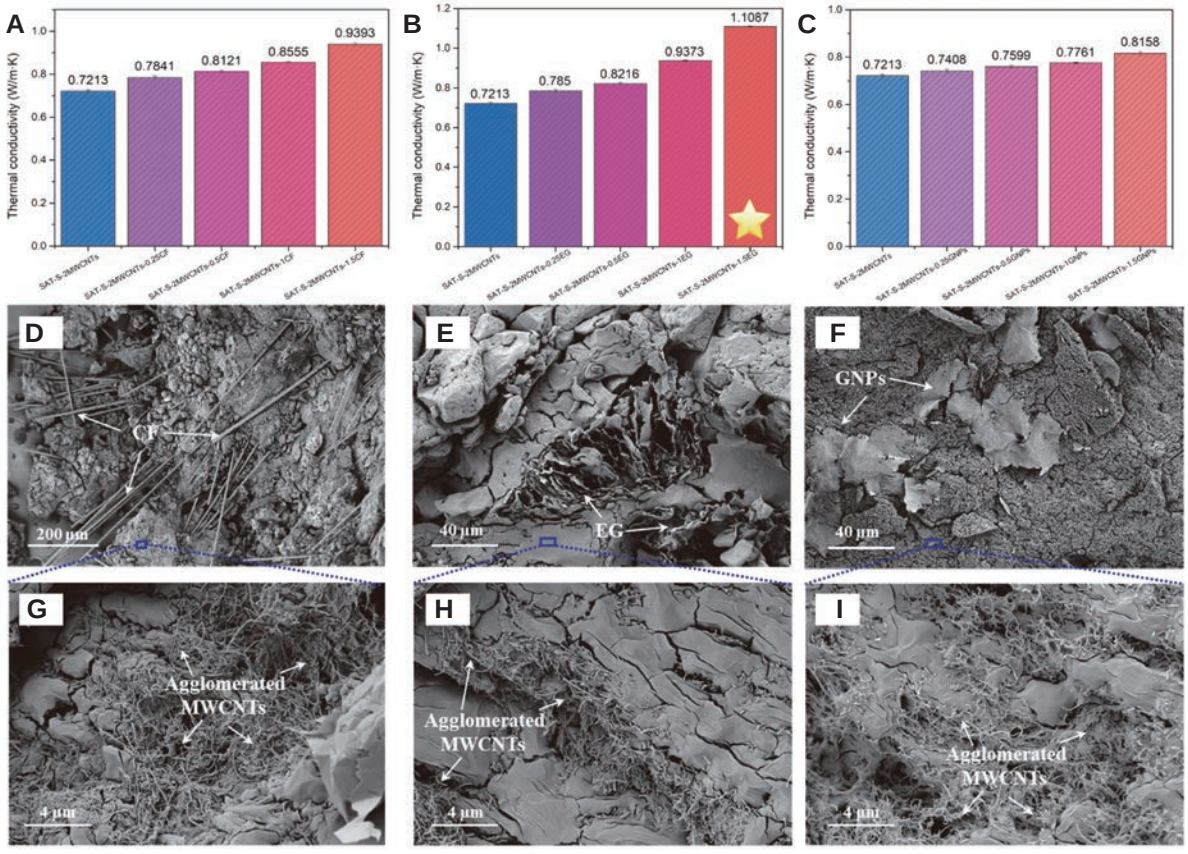

Figure 21 Enhancement of thermal conductivity through synergistic usage of carbon nanotube (1D additive) with carbon fiber (1D additive), expanded graphite (2D additive), and graphene nanoplates (2D additive). (A) Thermal conductivity enhancement by carbon nanotube and carbon fiber. (B) Thermal conductivity enhancement by carbon nanotube and expanded graphite. (C) Thermal conductivity enhancement by carbon nanotube and graphene nanoplates. Besides, SEM images of PCMs modified by different dimensions of carbon-based additives are shown in: (D) SAT-S-2MWCNTs-1.5CF 100 × and (G) 5000 ×, (E) SAT-S-2MWCNTs-1.5 EG 500 × and (H) 5000 ×, and (F) SAT-S-2MWCNTs-1.5GNPs 500 × and (I) 5000 × [5]. Copyright © 2022, Elsevier.

PCMs improved by 54.9%, while the photothermal conversion efficiency surged to 89.3% upon the incorporation of graphene nanoplates (2D additive) into the salt hydrate PCMs/carbon nanotubes (1D additive) composite, rendering it highly proficient in solar energy capture.

PHASE CHANGE TEMPERATURE

Phase change temperature is a critical factor in the design of PCM-enhanced building energy storage systems. These systems are expected to regulate heat on a diurnal scale, respond to short-term fluctuations like peak-valley electricity rates, and provide thermal or cooling energy over longer periods, accommodating seasonal variations in solar radiation and regional cold supply. As a result, PCMs must be tailored to meet the diverse temperature requirements outlined in Section of PCMs-ENHANCED BUILDING ENERGY STORAGE SYSTEMs.

To address these varying demands, binary mixtures, such as salt hydrates combined with organics or inorganic salts and ternary mixtures, are commonly employed to design and adjust PCMs with different phase change temperatures, as detailed in Table 10. For instance, in pursuit of a suitable PCM for air-conditioning cold storage, Zou *et al*. [123] introduced urea as a temperature-regulating agent. Their research demonstrated that the phase change temperature of $CaCl_2·6H_2O$ could be modulated, shifting from 9.5 to 29°C. They attributed this temperature adjustment to the presence of urea-generated amino groups, which weaken the interaction forces between $CaCl_2$ molecules and H_2O molecules, ultimately leading to a reduction in the phase change temperature. However, it is essential to note that not all temperature-regulating agents are universally compatible with all PCMs. As exemplified in Figure 22A. Fu *et al*. [124] reported unsatisfactory results when utilizing urea with $CH_3COONa·3H_2O$. The addition of urea resulted in the formation of two melting peaks and a significant reduction in the latent heat of $CH_3COONa·3H_2O$ when urea content exceeded 11%. Such alterations are undesirable in practical engineering applications. In light of these challenges, Yang *et al*. [5] introduced a novel temperature regulator, $NHCl_4$, into $CH_3COONa·3H_2O$. Their research showed that NH_4Cl could effectively tailor the phase change temperature of $CH_3COONa·3H_2O$, ranging from 57.5 to 45.1°C, making it adaptable to different application scenarios, as depicted in Figure 22B. However, it is crucial to exercise caution when employing NH_4Cl due to the potential adverse effects of its volatilized gas on human health.

Nonetheless, adjusting the melting point of salt hydrate PCMs through the use of temperature-regulating agents can also lead to a reduction in latent heat, as evident from the data presented in Table 10. Furthermore, the impact of varying agent contents can yield notably distinct outcomes even for identical salt hydrates. Therefore, in future endeavors involving the design of salt hydrate PCM-enhanced building energy storage systems, a critical consideration must be to ensure the preservation of a substantial latent heat capacity even when modifying the phase change temperature using these agents.

In addition to NH_4Cl, other potential temperature-regulating agents have been explored in the quest to tailor PCM phase change temperatures. Notably, Li *et al*. [56] introduced KCl as a candidate temperature-regulating agent. Their research, based on density functional theory calculations, revealed that K^+ ions could interact with CH_3COO^- ions by forming contact-ion pairs, weakening the interactions between anhydrous salts and water molecules, and thus reducing the phase change temperature [56,125]. However, it is important to note that the phase change temperature remained relatively constant when the KCl content exceeded 8 wt. %. Unfortunately, the lowest phase change temperature achieved for the SAT/KCl composite was 55°C, which was unsuitable for centralized energy storage systems. To address this issue, Li *et al*. [12] employed a ternary mixing approach. They incorporated an additional 3% urea into the mix, substantially reducing the phase-transition temperature of the binary SAT and KCl combination. This adjustment yielded a favorable

Table 10 Summary of temperature-regulated agents for virous salt hydrate PCMs

Salt hydrate PCMs	Temperature regulator	Volume of addition	Phase change temperature (°C)		Latent heat capacity (J/g)		Reference
			Original	After adjustive	Original	After adjustive	
$CaCl_2·6H_2O$	Urea (containing 5% ethanol, organics)	13%	29.0	11.0	–	134.9	[123]
		14%		11.2		120.1	
		15%		11.62		127.2	
		16%		9.54		104.8	
$CaCl_2·6H_2O$	Ethanol (containing 5% urea, organics)	2%	29.0	13.88	–	145.5	[123]
		3%		12.72		133.6	
		4%		11.58		113.3	
		5%		11.62		127.2	
		6%		7.98		96.31	
$CH_3COONa·3H_2O$	Urea (organics)	2%	58.17	56.20	266.5	262.7 (↓ 1.43%)	[124]
		5%		52.66		259.3 (↓ 2.70%)	
		8%		50.82		240.4 (↓ 9.79%)	
		11%		49.01		231.6 (↓ 13.1%)	
		15%		41.73		126.9 (↓ 52.38%)	
		17%		46.60		121.6 (↓ 54.37%)	
$CH_3COONa·3H_2O$	$NHCl_4$ (inorganic salt)	2.5%	57.5	51.7	250.2	–	[5]
		5%		49.9		–	
		7.5%		48.5		–	
		10%		45.1		172.2 (↓ 31.18%)	
$CH_3COONa·3H_2O$	KCl (inorganic salt)	2%	58.0	54.0	–	–	[56]
		4%		53.0		–	
		6%		52.0		–	
		8%		50.0		236.17	
		10%		50.0		–	
$CH_3COONa·3H_2O$	KCl/urea (inorganic salt/organics)	8%/3%	58.4	47.6	275.1	222.7 (↓ 19.05%)	[125]
$CH_3COONa·3H_2O$	Urea (containing 8% KCl, organics/inorganic salt)	1%	51.5	52.5	238.6	222.5 (↓ 6.75%)	[12]
		2%		49.7		239.8	
		3%		47.1		232.0 (↓ 2.77%)	
$CH_3COONa·3H_2O$	SiO_2 (containing 11% KCl, inorganics)	20%	48.45	43.50	240.4	164.0 (↓ 31.78%)	[126]
		25%		43.30		155.2 (↓ 35.44%)	
		30%		35.75		151.6 (↓ 36.94%)	
		35%		34.36		136.5 (↓ 43.22%)	

(*To be continued on the next page*)

(*Continued*)

Salt hydrate PCMs	Temperature regulator	Volume of addition	Phase change temperature (°C)		Latent heat capacity (J/g)		Reference
			Original	After adjustive	Original	After adjustive	
$CaCl_2·6H_2O$	Choline chloride (organics)	0.8:0.2 ($CaCl_2·6H_2O$:Choline chloride)	–	16.80	–	100.05	[69]
		0.86:0.14 ($CaCl_2·6H_2O$:Choline chloride)		20.65		127.22	
		0.89:0.11 ($CaCl_2·6H_2O$:Choline chloride)		23.05		135.21	
		0.91:0.09 ($CaCl_2·6H_2O$:Choline chloride)		24.10		146.57	
$CH_3COONa·3H_2O$	Formamide (organics)	0.75:0.25 ($CH_3COONa·3H_2O$:Formamide)	58.17	40.88	–	233.9	[127]
$CH_3COONa·3H_2O$	Tartaric acid (organics)	0.45:0.55 ($CH_3COONa·3H_2O$:Formamide)	58.4	50.00	264.3	209.3 (↓ 20.81%)	[94]
$CH_3COONa·3H_2O$	Glycine (organics)	3%	58.38	55.01	266.3	266.1 (↓ 0.08%)	[120]
		6%		52.88		265.0 (↓ 0.49%)	
		9%		51.09		261.8 (↓ 1.69%)	
		12%		48.62		258.5 (↓ 2.93%)	
		15%		48.67		256.0 (↓ 3.87%)	
		18%		48.38		251.9 (↓ 5.41%)	
		21%		48.34		246.4 (↓ 7.47%)	
$Mg(NO_3)_2·6H_2O$	$MgCl_2·6H_2O$ (eutectic salts)	35%	–	60.7	–	131.1	[128]
		50%		62.7		122.8	
$Na_2HPO_4·12H_2O$	$Na_2CO_4·10H_2O$ (eutectic salts)	9:1 ($Na_2HPO_4·12H_2O$:$Na_2CO_4·10H_2O$)	38.68	25.05	238.61	216.66 (↓ 9.20%)	[79]
		5:5 ($Na_2HPO_4·12H_2O$:$Na_2CO_4·10H_2O$)		26.94		198.44 (↓ 16.84%)	
		1:9 ($Na_2HPO_4·12H_2O$:$Na_2CO_4·10H_2O$)		25.66		173.95 (↓ 27.10%)	
$CaCl_2·6H_2O$	$MgCl_2·6H_2O$ (eutectic salts)	10%	–	26.0	–	–	[129]
		15%		25.0		–	
		20%		23.5		–	
		25%		21.0		–	

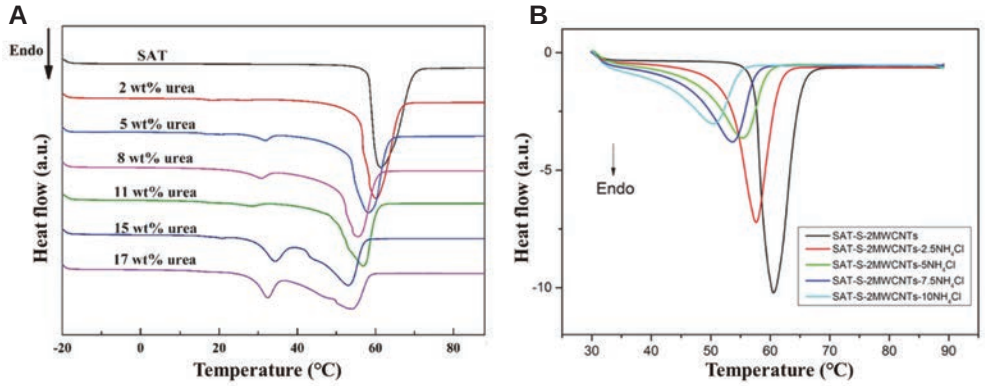

Figure 22 Differential scanning calorimetry curves of $CH_3COONa{\cdot}3H_2O$ with different temperature regulators. (A) Urea [124] and (B) $NHCl_4$ [5]. Copyright © 2018, Elsevier, Copyright © 2022, Elsevier.

phase change temperature of 47.8°C and a higher latent heat of 242.0 J/g.

Furthermore, another technique known as the eutectic salt method involves adding a certain proportion of another hydrated salt to the base hydrated salt to create a eutectic hydrated salt, effectively altering the melting point. Rao *et al*. [79] and Xie *et al*. [81] showcased the efficacy of this method in crafting salt hydrates with distinct phase change temperatures. For instance, when the ratio of $Na_2SO_4{\cdot}10H_2O$ to $Na_2CO_3{\cdot}10H_2O$ was adjusted to 1:1, the resulting eutectic salt hydrate displayed a phase-transition temperature of approximately 26°C. This value was lower than that of both individual salt hydrates, making it suitable for passive-construction thermal storage systems, such as thermoregulated wall and floor components, as illustrated in Figure 4.

CORROSION TO METALS

Metal materials are often favored for macro-encapsulation of PCMs due to their desirable properties, including resistance to wear, high thermal conductivity, ductility, and overall durability. However, the issue of corrosion poses a significant challenge to the safe and cost-effective application of TES systems involving most salt hydrates [92]. This is primarily because metal materials tend to corrode upon contact with salt hydrates, effectively serving as an electrolyte solution. Consequently, various techniques, such as gravimetric analysis and microscopic observation, as well as industry standards (ASTM G1–03) [130–132], have been developed to calculate the corrosion rate (CR, calculated by Eqs. (23) and (24)) of metal materials. Additionally, classification guidelines have been established to provide clear guidance, as outlined in Table 11. In practical applications, metal materials must exhibit corrosion resistance, with the CR being less than 9.9 mg/(cm^2 a).

$$\Delta m = m(t_0) - m(t), \tag{23}$$

$$\mathrm{CR} = \Delta m / A_c \cdot (t_0 - t), \tag{24}$$

where Δm, $m(t_0)$, and $m(t)$ denote the mass loss, initial mass, and mass measured at a specific time, respectively; A_c denotes the area in cm^2, and t_0 and t are the initial and related times, respectively.

Table 12 overviews the different metal materials employed with various salt hydrates. For instance,

Table 11 Industry standard for corrosion weight loss measurement guideline [130–132]

Corrosion rate (mg/(cm^2 a))	Corrosion depth (mm/a)	Recommendation
>1000	2	Completely destroyed within days
100–999	0.1–1.99	Not recommended for service greater than a month
50–90	0.1–0.19	Not recommended for service greater than 1 year
10–49	0.02–0.19	Caution recommended, based on the specific application
0.3–9.9	–	Recommended for long-term service
<0.2	–	Recommended for long-term service; no corrosion, other than as a result of surface cleaning, was evidenced

Table 12 Corrosion performance of metals for long-term encapsulation of various salt hydrate PCMs

Metals	Recommended to encapsulate salt hydrates	Corrosion rate (mg/(cm^2 a))	Reference
Aluminum alloy AA6061	$Mg(NO_3)_2·6H_2O$	–	[133]
Aluminum alloy	$Mg(NO_3)_2·6H_2O$	2.3	[134]
Carbon steel	Mixture of $Mg(NO_3)_2·6H_2O$ and $Ca(NO_3)_2·4H_2O$	4.6	[135]
Stainless steel	$NaSO_4·10H_2O$; $ZnCl_2·3H_2O$; $NaOH·1.5H_2O$; $K_2HPO_4·6H_2O$; $MgSO_4·7H_2O$; $CH_3COONa·3H_2O$; $Zn(NO_3)_2·4H_2O$;	Lower than 1.0	[131]
Stainless steel 316	Mixture of $Na_2HPO_4·12H_2O$ and $Na_2SO_4·10H_2O$	–	[136]
Stainless steel 316	$CaCl_2·6H_2O$	–	[132]
Stainless steel 316	$CaCl_2·6H_2O$; $Na_2S·5H_2O$; $Ca(OH)_2$; $MgCl_2·6H_2O$; $MgSO_4·7H_2O$	Lower than 9.9	[137]
Stainless steel	$CH_3COONa·3H_2O$	Lower than 0.4	[138]

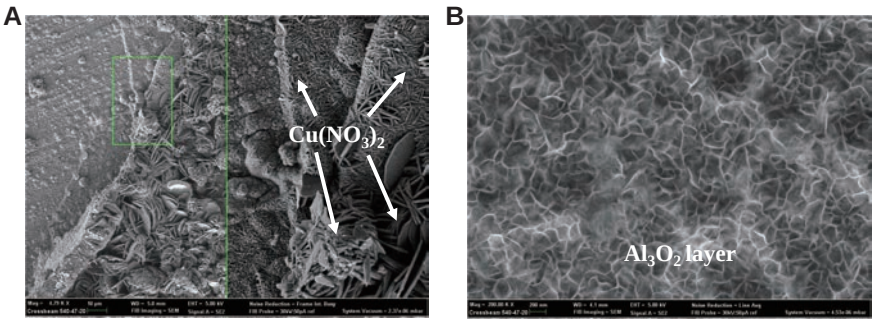

Figure 23 SEM images of the corroded surface of (A) copper alloy and (B) aluminum alloy after 7 days' corrosion in $Mg(NO_3)_2·6H_2O$ at 120°C [133]. Copyright © 2019, Elsevier.

Calabrese *et al*. [133] noted that copper and aluminum alloy surfaces displayed varying degrees of degradation after 7 days of corrosion in $Mg(NO_3)_2·6H_2O$ liquid. Copper alloy surfaces exhibited numerous Cu $(NO_3)_2$ crystal corrosion products, while aluminum alloy surfaces showed minimal signs of corrosion, featuring only a thin Al_2O_3 layer (commonly referred to as a passivation film), as illustrated in Figure 23. As a result, they concluded that aluminum alloy, in comparison to copper alloys, is a more suitable and effective material for coating $Mg(NO_3)_2·6H_2O$ containers. Subsequently, Honcova *et al*. [134] corroborated these findings, reporting a CR of 2.3 mg/(cm^2 a) for aluminum alloy in $Mg(NO_3)_2·6H_2O$ liquid, which falls well below the industry standard of 9.9 mg/(cm^2 a).

Moreover, according to research conducted by Devanuri *et al*. [138], stainless steel demonstrates remarkable resistance to corrosion from virtually all hydrated inorganic salts. This exceptional resistance is attributed to the presence of 15% chromium in stainless steel. Chromium, compared with other elements, has

a superior ability to form an oxide (passivation) film. This film acts as a protective barrier, effectively isolating the metal from external inorganic salts and preventing further corrosion. In the event of damage, chromium can regenerate this protective passivation film, ensuring long-term durability. As a result, stainless steel plays a crucial role in enhancing the corrosion resistance of salt hydrates. However, Cabeza *et al*. [139,140] caution against the indiscriminate use of stainless steel for long-term encapsulation of hydrated chloride. While no corrosion was observed during their testing period, stainless steel remained at a high risk of contact with chloride ions. Specifically, stainless steel may accelerate corrosion due to the unique characteristics of chloride ions, such as their small ion radius and strong penetration ability. These ions can preferentially adsorb onto the passivated iron carbonate film, leading to pitting, stress, and crevice corrosion. The volume deformation of the PCMs, occurring before and after the phase change, can also influence the shape of the container, exacerbating its deterioration. Therefore, evaluating strip specimens alone may not provide a complete picture. Metal materials must be configured into container shapes to accurately assess whether the metal container's deformation affects its CR. Because existing investigations rely on laboratory test methods, studies have been scarce monitoring the practical application of stainless steel with salt hydrates over the past decades. Consequently, stainless steel has not been widely adopted for encapsulating salt hydrates. Long-term studies using practical measurements are imperative in the future to gather more reliable data.

Additionally, various measures can be implemented to mitigate corrosion and meet specific application requirements. The sacrificial anode strategy [141], commonly employed in engineering applications to prevent steel bar corrosion in bridge columns, can also be applied in this context. Furthermore, galvanizing the metal surface represents another effective approach. Coating a non-metallic protective or barrier layer on the metal surface is an excellent choice for isolating the metal from salt hydrates. However, it is noteworthy that, to date, researchers have not extensively explored the impact of salt hydrates on the corrosion resistance of various metal surface modifications.

APPLICATIONS OF SALT HYDRATE PCMS FOR BUILDING

The application of salt hydrates as PCMs for building energy storage systems can be divided into three categories, including PCMs-enhanced facilities, PCMs-enhanced building envelopes, and PCMs-enhanced geostructures. These applications are envisioned to facilitate diurnal heat regulation in the short term and provide thermal energy or cold energy distribution over the course of months or even seasons in the long term.

Facilities

Building facilities primarily encompass heating, ventilating, and air conditioning systems, often abbreviated as HVAC. Farid *et al*. [142] categorize PCMs into materials for storage of coolness in air conditioning applications ($T_m < 15$°C), materials for absorption refrigeration ($T_m > 90$°C), and materials for solar heating and related applications (15°C < T_m < 90°C). Zeinelabdein *et al*. [128] reviewed various free cooling technologies for ventilating and air conditioning systems, highlighting the promising sustainability of using

PCMs to minimize energy consumption. They emphasized the potential of night cooling strategies employing PCMs to effectively maintain indoor temperatures within the comfort zone while substantially reducing cooling loads across a range of climates. Moreover, for heating systems, the temperature characteristics of salt hydrate PCMs lend themselves to a variety of applications. These include solar water heating [143–145], solar drying [16,146,147], photothermal /photovoltaic systems [148,149], waste heat recovery [150], and other related fields.

Notably, as depicted in Figure 24A, solar water heating systems are particularly favored in regions with temperate, arid, and tropical climates. These systems can be categorized as PCM-enhanced integrated and PCM-enhanced non-integrated systems [145]. In non-integrated solar collectors, the separation of PCM mass from the solar collector provides greater design flexibility, allowing for increased PCM utilization and compatibility with various external systems. For instance, Kılıçkap *et al*. [144] integrated salt hydrate PCMs with a hot water collector and conducted tests in Turkey. In their investigation, the hot water collector containing $CaCl_2{\cdot}6H_2O$ exhibited the highest heat collection efficiency, extending the availability of hot water at the desired temperature by 1–1.5 h. Additionally, Ding *et al*. [143] assessed the power-saving and heat loss reduction rates in solar water heating systems, both with and without PCMs, across six cities in China (Lhasa, Kunming, Shenyang, Zhengzhou, Changsha, and Guangzhou). Their findings indicated that Lhasa exhibited the highest power-saving rate, while Guangzhou demonstrated the most significant heat loss reduction rate.

Moreover, the drying of agricultural products is emerging as a new trend in PCM applications, particularly when moderate and consistent temperatures are required during the drying process [16]. Drying processes are known to be energy-intensive within the food industry. Recent research by Madhankumar *et al*. [146] combined solar drying devices with PCMs to efficiently dry agricultural products using solar energy, as shown in Figure 24B. Their study revealed that PCMs equipped with fins substantially reduced specific energy consumption, accelerated moisture drying, and yielded robust, high-quality agricultural products.

Building envelopes

The integration of PCMs into the building envelope helps with building thermal management (e.g., peak heat flux reduction and time delay) as well as in reducing building energy consumption, which stands out as a promising approach. This innovation enables the regulation of room temperatures, maintaining them within the thermal comfort range of 20–28°C, and facilitates the harnessing of solar energy (with the capability to meet hot water demand in the range of 29–68°C) within buildings.

A comprehensive long-term real-size study was conducted by Sonnick *et al*. [151] to investigate the impact of a salt-hydrate mixture comprising $CaCl_2{\cdot}6H_2O$ and $MgCl{\cdot}6H_2O$ on the thermal performance of a lightweight building, utilizing a prefabricated wooden house as a representative model, as shown in Figure 25A. The results demonstrated that, in comparison to a reference room, the building enhanced with PCMs exhibited a remarkable 57% reduction in overall temperature fluctuations and a substantial 62% reduction in day-night temperature swings. Additionally, Bao *et al*. [68] employed numerical analysis techniques to simulate the indoor temperature variations within building envelopes in Hong Kong and Changsha, applying modified $CaCl_2{\cdot}6H_2O$ salt hydrate PCMs. As shown in Figure 25B, their findings underscored the efficacy of PCMs in effectively moderating indoor temperatures, contributing to more energy-efficient and comfortable

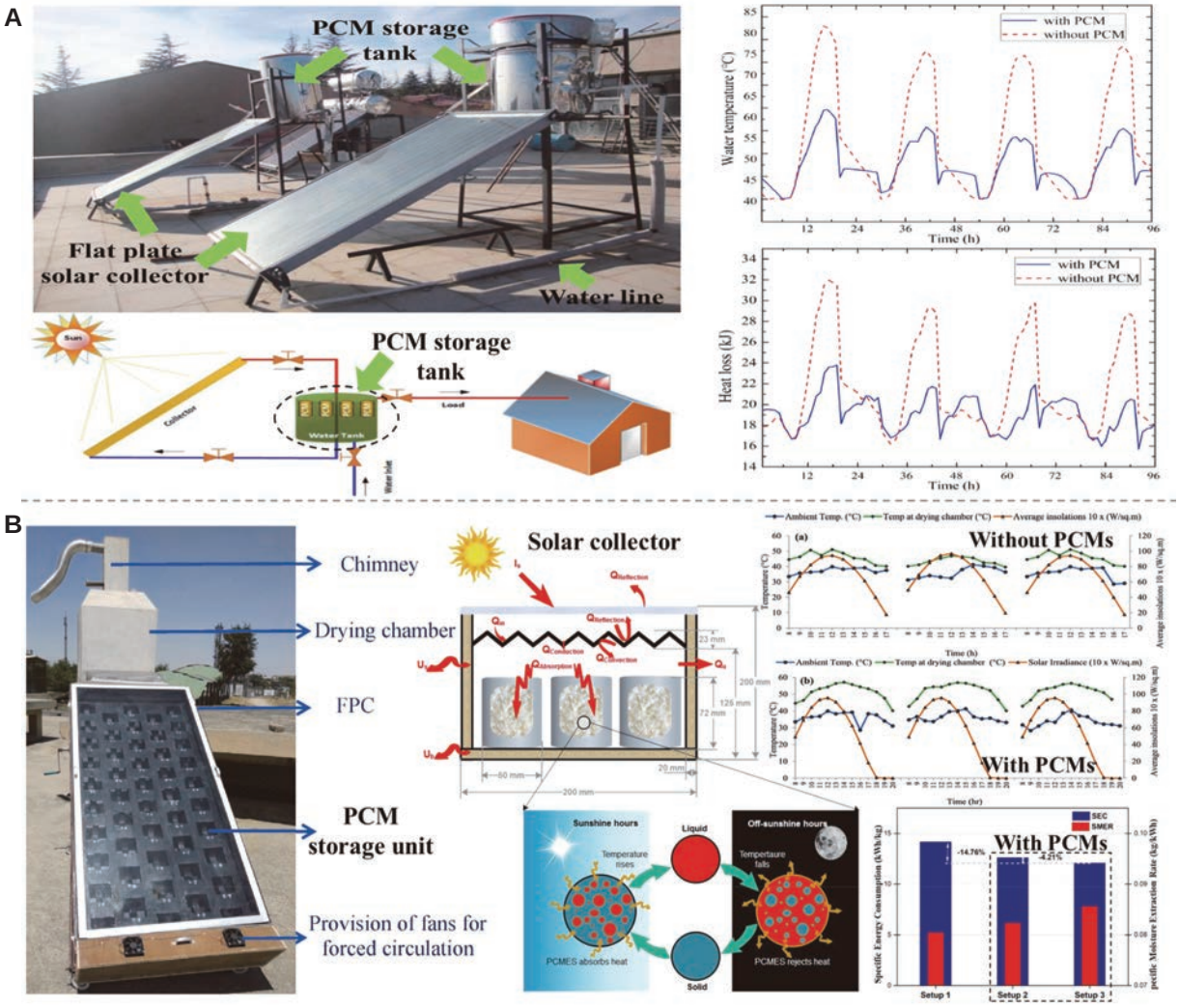

Figure 24 Applications of salt hydrate PCMs in solar energy storage and utilization. (A) Solar water heating, adapted with permission from references [143–145], Copyright © 2020, Elsevier, Copyright © 2018, Elsevier, Copyright © 2021, Elsevier, and (B) solar drying, adapted with permission from references [16,146,147], Copyright © 2014, Elsevier, Copyright © 2023, Elsevier, Copyright © 2021, Elsevier.

building environments.

Besides, de Gracia *et al*. [153] employed the life cycle assessment methodology to scrutinize the environmental impact of PCM usage, comparing organic PCMs with salt hydrate PCMs in Mediterranean constructions, as depicted in Figure 26A. The results indicate that the utilization of salt hydrate PCMs reduces the environmental impact associated with manufacturing and allows for a shorter-term payback compared with organic PCMs, with payback times of 25 and 61 years for salt hydrate PCMs and organic PCMs, respectively. Additionally, Mukhamet *et al*. [154] conducted a comprehensive evaluation of PCMs for building envelope applications, utilizing a multi-criteria decision-making approach, as shown in Figure 26B. In their study, the total annual energy savings of commercial salt hydrate PCMs S27 far exceeded that of other PCMs. And the S27 used in Bamako has an energy saving of approximately 8392 kWh and a 43% reduction in energy consumption. They then ranked various PCMs, including salt hydrate PCMs, organic

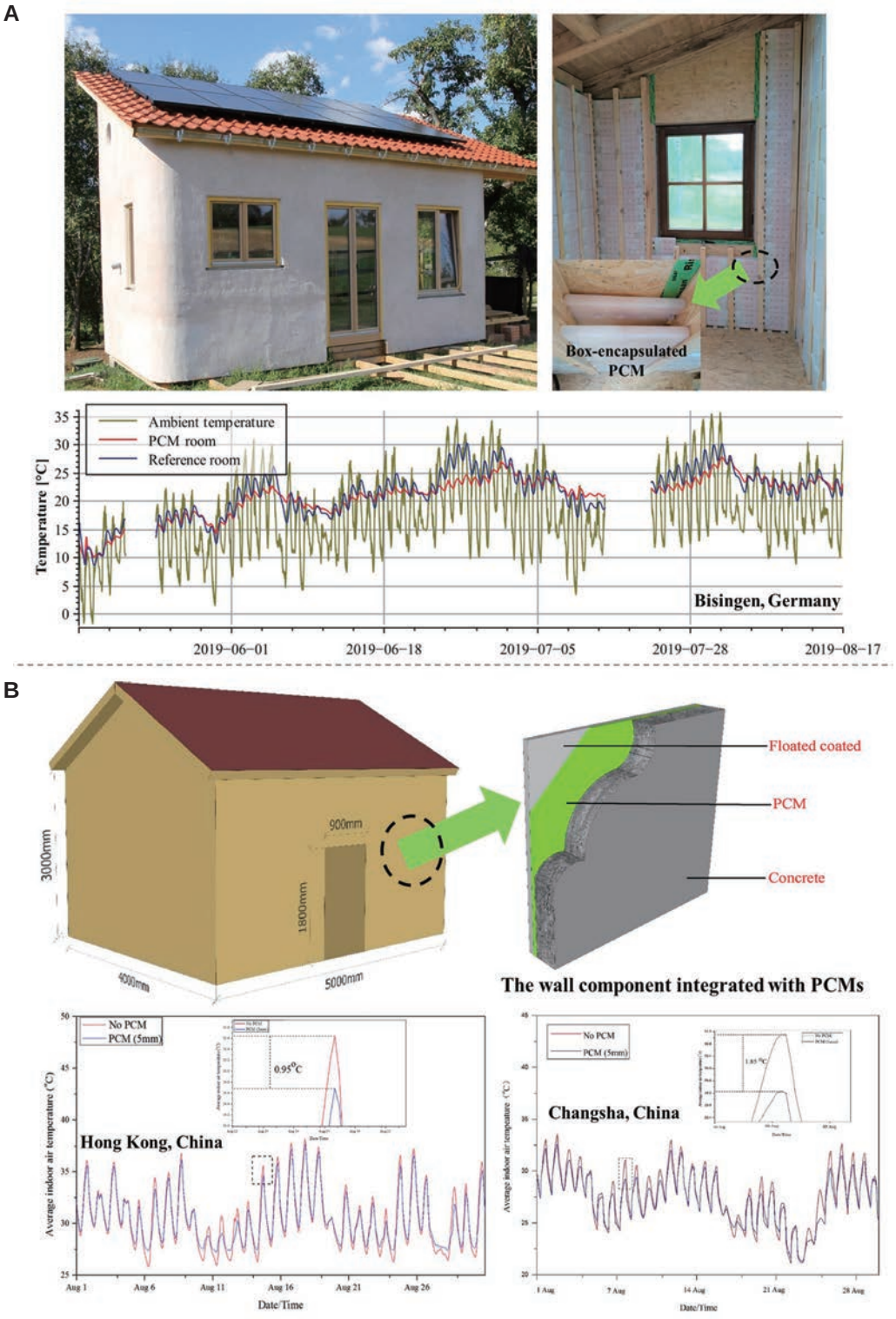

Figure 25 Applications of salt hydrate PCMs in building envelopes. (A) A long-term real size experiment using salt hydrate PCMs [151,152], Copyright © 2020, Wiley, Copyright © 2018, Elsevier. (B) Numerical simulation of house integrated with salt hydrate PCMs [68], Copyright © 2020, Elsevier.

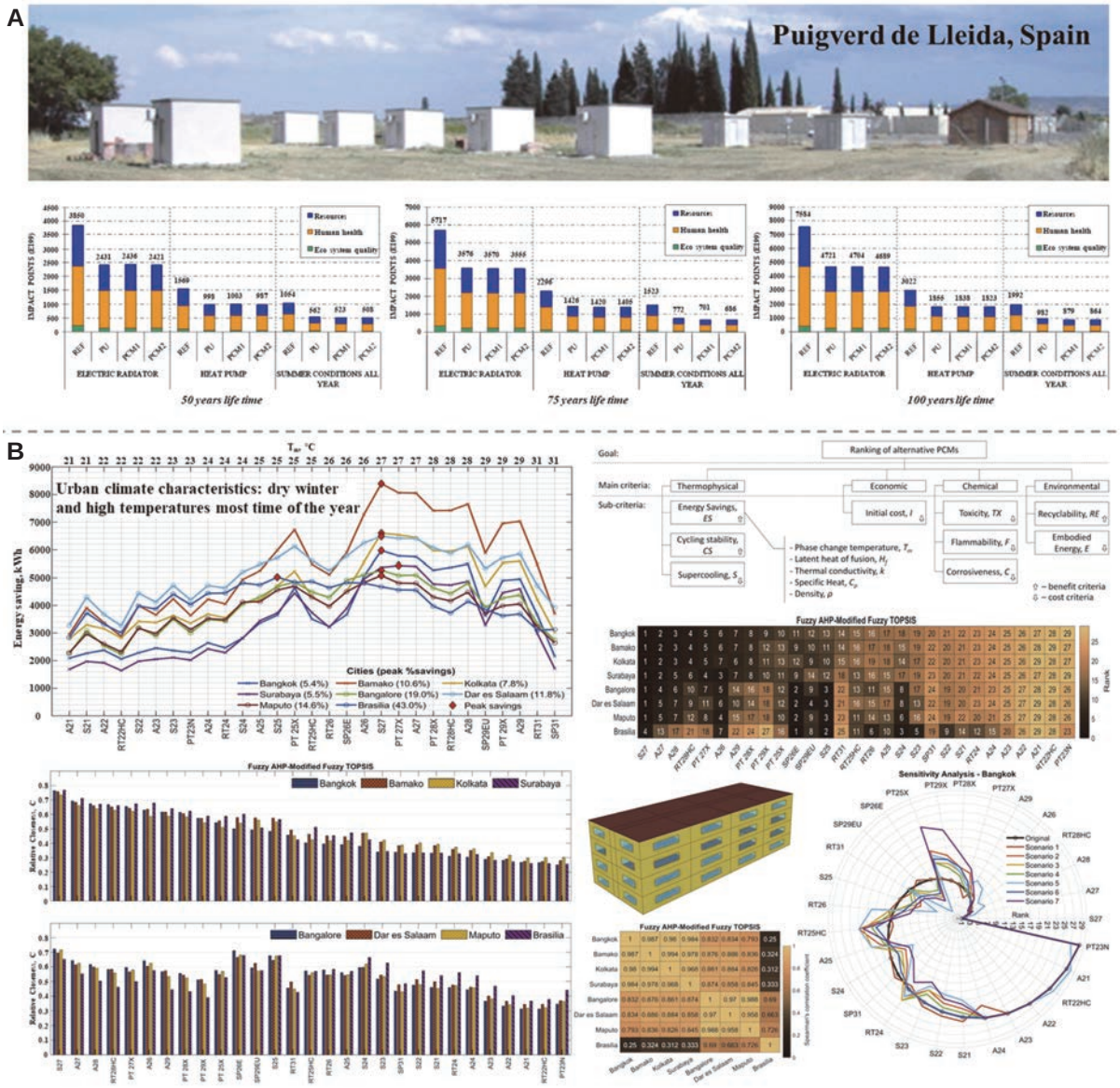

Figure 26 Comparative study of organic PCMs and salt hydrate PCMs applied in building envelopes. (A) The life Cycle Assessment [153] (PCM1 and PCM2 denote organic PCMs and salt hydrate PCMs, respectively), Copyright © 2010, Elsevier. (B) The multi-objective ranking via Fuzzy AHP-Modified Fuzzy TOPSIS method [154] (S and SP both denote salt hydrate PCMs; A and RT both denote organic PCMs; PT denotes biobased PCMs), Copyright © 2021, Elsevier.

PCMs, and biobased PCMs, using the Fuzzy AHP-Modified Fuzzy TOPSIS method. Factors considered in the evaluation encompassed thermophysical (thermal conductivity, latent heat of fusion, phase change temperature, specific heat, density, cycling stability, supercooling), economic (initial cost), chemical (toxicity, flammability, corrosiveness), and environmental (recyclability, embodied energy) aspects. According to their study, salt hydrate PCMs are more suitable for savanna climate buildings than organic and biobased PCMs due to high energy savings, low cost, non-flammability, high latent heat energy, and their consistently high-ranking position in the sensitivity analysis.

Geostructures

Shallow geothermal energy stands as a sustainable and eco-friendly resource that can effectively power heating and cooling systems within buildings. The integration of ground source heat pumps (GSHP) with geostructures, such as energy tunnels [155], energy pile [156], and energy diaphragm wall [157], has emerged as a practical solution. Recently, the incorporation of PCMs into these structures to enhance heat storage density has gained prominence, as illustrated in Table 13.

Alavy *et al*. [158] developed a thermal caisson by integrating PCMs into energy piles, investigating their impact on the COP of the heat pump system. Results showed that combining PCMs with energy piles improved GSHP system performance by up to 16%, while, without the need for additional drilling, they reduced capital costs by up to 49%. In another study [159], the authors evaluated the influence of PCMs and ordinary backfill materials on the heat transfer performance of precast high-strength concrete energy piles. They suggested that PCMs with a larger latent heat, higher thermal conductivity, and lower melting temperature (under the cooling mode) can enhance the heat transfer performance of energy piles. Furthermore, Mousa *et al*. [160] explored the feasibility of using PCMs as a thermal storage system in energy piles. Their study recommended partitioning the PCM into smaller containers, noting that while adding PCMs as a whole increased the COP of the heat pump in the energy pile by approximately 5.28%, further partitioning the PCMs into smaller containers raised the COP by about 26%.

Recently, the TES concrete [4,7,169–171], renowned for its high heat storage density achieved through the effective integration of concrete and PCMs, has begun to establish itself in the realm of energy geostructures. In this energy pile system, PCMs are divided into small units, and the encapsulated PCM is uniformly distributed in the pile body as coarse aggregate. Cui's group [161] conducted a comparative analysis of the thermo-mechanical performance of an ordinary pile and a PCM energy pile in saturated sand. Their study revealed that the strain of the PCMs energy pile was 2% smaller than that of the ordinary energy pile, and the displacement was reduced by 6%, effectively enhancing the durability of the energy pile. Furthermore, Bao *et al*. [8] investigated the thermal response of a PCM energy pile in unsaturated clay. The results indicated that, compared with the traditional energy pile, the temperature of the PCM energy pile is more uniform, and the heat transfer power of the PCM energy pile is higher. Although research on the combination of PCMs and energy geostructures is flourishing, the exploration of salt hydrate PCMs in energy geostructure lags behind that of organic PCMs, with only a few scholars [166,167] participating.

CONCLUSIONS AND RECOMMENDATIONS

This review provided a comprehensive overview of the progress and challenges associated with salt hydrate PCMs in enhancing building energy storage systems. Through critical analysis, this review identified several key issues concerning salt hydrates and explored optimization methods and underlying mechanisms. The following conclusions have been drawn.

(1) Salt hydrates, with their inherent advantages such as non-flammability, high enthalpy, and cost-effectiveness, hold promising prospects for applications in energy storage systems within the construction sector. While solutions to common challenges like supercooling, phase separation, and low thermal con-

Table 13 Summary of energy geostructures integrated with PCMs

Structure element	Type of PCM	PCM characteristics	PCM utilization pattern	Research methodology	Reference
Energy pile	RT2HC	1–3°C, 200 J/g	PCM pipes *29 (around the perimeter)	PCM analysis System COP analysis Results validation Cost analysis	[158]
Energy pile	$CaCl_2 \cdot 6H_2O$	28°C, 200 J/g	PCM backfill	Effects of PCM properties on thermal performance of PHC energy pile Effect of different backfill materials on thermal performance of PHC energy pile Effect of different operation patterns on thermal performance of PHC energy pile Effect of groundwater seepage on thermal performance of PHC energy pile	[159]
Energy pile	RT5HC	4–6°C, 250 J/g	PCM tubes *4 (around the center)	Energy pile performance without a PCM PCM temperature and phase profiles Effect of a PCM on the GSHP performance Effect of a PCM on the thermal radius Effect of the PCM location on the GSHP performance Effect of the melting temperature Effect of using multiple PCM melting temperatures	[160]
Energy pile	Paraffin	23±1°C, 188 J/g	PCM aggregates (coarse aggregates replacement)	Horizontal temperature change Temperature change with depth Phase transition progression inside the pile Temperature distribution in pile-soil Heat power; pile-soil displacement Pile internal stress and side friction Thermo-mechanical response behavior of the FRPC pile	[161,162]
Energy pile	Paraffin	23±1°C, 188 J/g	PCM aggregates (coarse aggregates replacement)	Water temperatures of the inlet and outlet Temperature distribution Thermal response of the soil Influence of operation modes Heat transfer power	[8,163]
Energy pile	MicroPCM	28.7°C, 180 J/g	PCM additives	Mechanical and thermal properties of MicroPCM C50 concrete Energy performance of MicroPCM energy pile	[164]
Energy pile	Lauric acid	43.5–48.2°C, 187 J/g	PCM tube *1 (in the center)	Effects of the PCM on the thermal response of the pile body Observing the phase change process Effects of the PCM on the thermal response of the soil media Effects of the PCM on the thermal-induced excess pore water pressures Effects of the PCM on the power output	[165]
Energy pile	Salt hydrates	22.9°C, 200 J/g	Round PCM sheet (around the perimeter)	Model validation Preliminary performance and economic analysis	[166]
Energy pile	Salt hydrates	22.9°C, 200 J/g	Round PCM sheet (around the perimeter)	Outlet fluid temperature and phase change process Temperature profiles in the water tank and soil	[167]
Energy tunnel	–	15°C, 182 J/g	PCM plates	Effect of PCM thermal conductivity on cold energy storage of PCM plate Effect of PCM melting temperature on cold energy storage of PCM plate Effect of surrounding rock temperature on cold energy storage of PCM plate Effect of tunnel lining GHEs length on cold energy storage of PCM plate	[168]

ductivity are emerging, further research is essential. Notably, the adoption of salt hydrates in practical applications still lags behind that of organic PCMs.

(2) Nanomaterials represent a potential solution to mitigating supercooling in salt hydrates. Their nanoscale size closely aligns with the critical nucleation radius, significantly reducing the heterogeneous nucleation barrier. However, widespread production of nanomaterial-modified salt hydrates may present challenges due to the need for ultrasonic dispersion and relatively high costs. Future research should focus on exploring efficient methods for supercooling inhibition.

(3) Various technologies, including thickening, gelling, porous-carrier absorption, and microencapsulation, have proven effective in preventing phase separation of salt hydrates. Nevertheless, there is a need for long-term cycle stability assessments and a deeper understanding of the underlying mechanisms, particularly for microencapsulation. In the future, innovative solutions with self-healing capabilities should be developed to address stability issues after multiple cycles. Furthermore, the use of porous carriers for salt hydrate absorption presents a straightforward and efficient method for overcoming phase separation. Consequently, research into developing porous supports with high thermal conductivity and porosity to accommodate salt hydrates is poised to become a prominent area of study.

(4) 3D thermal enhancers have demonstrated a remarkable ability to enhance the thermal conductivity of salt hydrates, outperforming their 2D, 1D, and 0D counterparts. Future research should explore the synergistic use of enhancers with different dimensions to develop salt hydrates with even higher thermal conductivity. Leveraging machine learning techniques can prove instrumental in predicting variations in the phase change temperature of salt hydrates and facilitating the design of salt hydrates with specific phase change temperatures.

(5) The phase change temperature of salt hydrate PCMs can be fine-tuned by incorporating temperature-regulated agents, such as organic materials, other types of salts, or salt hydrates. This adjustment widens the application range of salt hydrate PCMs across diverse fields. However, it is imperative to note that the introduction of temperature regulators often results in a reduction of latent heat capacity. In future designs of salt hydrate PCMs-enhanced building energy storage systems, ensuring substantial latent heat capacity while adjusting the phase change temperature is essential.

In conclusion, salt hydrate PCMs hold great promise for revolutionizing building energy storage systems. To fully harness their potential, continued research, innovation, and practical applications are vital. Addressing the identified challenges and further optimizing these remarkable materials will drive the advancement of sustainable and energy-efficient building solutions.

Data availability

The original data are available from the corresponding authors upon reasonable request.

Funding

This work was supported by the National Natural Science Foundation of China (51925804 and 52208275) and the China Postdoctoral Science Special Foundation (2023T160433).

Author contributions

H.Y. and Y.Z. collated and summarized the literature and wrote the manuscript. H.C. guided the manuscript. All authors

discussed and commented on the manuscript.

Conflict of interest

The authors declare no conflict of interest.

References

1 Wang Z, Li H, Zhang B, *et al.* Unequal residential heating burden caused by combined heat and power phase-out under climate goals. *Nat Energy* 2023; **8**: 881–890.

2 You K, Li R, Yu Y, *et al.* Investigating CO_2 emissions and disparity from China's central heating: A perspective at the city level. *Environ Impact Assessment Rev* 2023; **103**: 107270.

3 Guan X, Guo S, Xiong J, *et al.* Energy-related CO_2 emissions of urban and rural residential buildings in China: A provincial analysis based on end-use activities. *J Building Eng* 2023; **64**: 105686.

4 Cui H, Zou Y, Yang H, *et al.* Thermal-mechanical behaviors of concrete with innovative salt hydrate PCM-based thermal energy storage aggregate. *Energy Convers Manage* 2023; **293**: 117477.

5 Yang H, Bao X, Cui H, *et al.* Optimization of supercooling, thermal conductivity, photothermal conversion, and phase change temperature of sodium acetate trihydrate for thermal energy storage applications. *Energy* 2022; **254**: 124280.

6 Islam MM, Pandey AK, Hasanuzzaman M, *et al.* Recent progresses and achievements in photovoltaic-phase change material technology: A review with special treatment on photovoltaic thermal-phase change material systems. *Energy Convers Manage* 2016; **126**: 177–204.

7 Yang H, Xu Z, Cui H, *et al.* Cementitious composites integrated phase change materials for passive buildings: An overview. *Constr Build Mater* 2022; **361**: 129635.

8 Bao X, Qi X, Cui H, *et al.* Experimental study on thermal response of a PCM energy pile in unsaturated clay. *Renew Energy* 2022; **185**: 790–803.

9 Zhang G, Cao Z, Xiao S, *et al.* A promising technology of cold energy storage using phase change materials to cool tunnels with geothermal hazards. *Renew Sustain Energy Rev* 2022; **163**: 112509.

10 Said MA, Hassan H. Parametric study on the effect of using cold thermal storage energy of phase change material on the performance of air-conditioning unit. *Appl Energy* 2018; **230**: 1380–1402.

11 Shan K, Fan C, Wang J. Model predictive control for thermal energy storage assisted large central cooling systems. *Energy* 2019; **179**: 916–927.

12 Li M, Lin Z, Sun Y, *et al.* Preparation and characterizations of a novel temperature-tuned phase change material based on sodium acetate trihydrate for improved performance of heat pump systems. *Renew Energy* 2020; **157**: 670–677.

13 Jin X, Wu F, Xu T, *et al.* Experimental investigation of the novel melting point modified Phase-Change material for heat pump latent heat thermal energy storage application. *Energy* 2021; **216**: 119191.

14 Li SF, Liu Z, Wang XJ. A comprehensive review on positive cold energy storage technologies and applications in air conditioning with phase change materials. *Appl Energy* 2019; **255**: 113667.

15 Hofer G, Kotik J, Pröll T. Heat loss reduction and tap temperature equalization of a centralized domestic hot water system in a modernized pre-WWI residential building. *J Building Eng* 2023; **77**: 107506.

16 Shalaby SM, Bek MA, El-Sebaii AA. Solar dryers with PCM as energy storage medium: A review. *Renew Sustain Energy Rev* 2014; **33**: 110–116.

17 Sani AK, Singh RM, Amis T, *et al.* A review on the performance of geothermal energy pile foundation, its design process and applications. *Renew Sustain Energy Rev* 2019; **106**: 54–78.

18 Cabeza LF, Castell A, Barreneche C, *et al.* Materials used as PCM in thermal energy storage in buildings: A review. *Renew Sustain Energy Rev* 2011; **15**: 1675–1695.

19 Wong-Pinto LS, Milian Y, Ushak S. Progress on use of nanoparticles in salt hydrates as phase change materials. *Renew Sustain Energy Rev* 2020; **122**: 109727.

20 Beaupere N, Soupremanien U, Zalewski L. Nucleation triggering methods in supercooled phase change materials (PCM), a review. *Thermochim Acta* 2018; **670**: 184–201.

21 Zahir MH, Mohamed SA, Saidur R, *et al.* Supercooling of phase-change materials and the techniques used to mitigate the phenomenon. *Appl Energy* 2019; **240**: 793–817.

22 Kumar N, Hirschey J, LaClair TJ, *et al.* Review of stability and thermal conductivity enhancements for salt hydrates. *J Energy Storage* 2019; **24**: 100794.

23 Schmit H, Rathgeber C, Hoock P, *et al.* Critical review on measured phase transition enthalpies of salt hydrates in the context of solid-liquid phase change materials. *Thermochim Acta* 2020; **683**: 178477.

24 Yu K, Liu Y, Yang Y. Review on form-stable inorganic hydrated salt phase change materials: Preparation, characterization and effect on the thermophysical properties. *Appl Energy* 2021; **292**: 116845.

25 Liu H, Wang W, Zhang Y. Performance gap between thermochemical energy storage systems based on salt hydrates and materials. *J Cleaner Production* 2021; **313**: 127908.

26 Hua W, Lv X, Zhang X, *et al.* Research progress of seasonal thermal energy storage technology based on supercooled phase change materials. *J Energy Storage* 2023; **67**: 107378.

27 Dannemand M, Dragsted J, Fan J, *et al.* Experimental investigations on prototype heat storage units utilizing stable supercooling of sodium acetate trihydrate mixtures. *Appl Energy* 2016; **169**: 72–80.

28 Johansen JB, Dannemand M, Kong W, *et al.* Thermal conductivity enhancement of sodium acetate trihydrate by adding graphite powder and the effect on stability of supercooling. *Energy Procedia* 2015; **70**: 249–256.

29 Li X, Zhang J, Liu Y, *et al.* Supercooled sugar alcohols stabilized by alkali hydroxides for long-term room-temperature phase change solar-thermal energy storage. *Chem Eng J* 2023; **452**: 139328.

30 Zhou G, Xiang Y. Experimental investigations on stable supercooling performance of sodium acetate trihydrate PCM for thermal storage. *Sol Energy* 2017; **155**: 1261–1272.

31 Ling Z, Luo M, Song J, *et al.* A fast-heat battery system using the heat released from detonated supercooled phase change materials. *Energy* 2021; **219**: 119496.

32 Dannemand M, Kong W, Fan J, *et al.* Laboratory test of a prototype heat storage module based on stable supercooling of sodium acetate trihydrate. *Energy Procedia* 2015; **70**: 172–181.

33 Wang G, Xu C, Kong W, *et al.* Review on sodium acetate trihydrate in flexible thermal energy storages: Properties, challenges and applications. *J Energy Storage* 2021; **40**: 102780.

34 Eanest Jebasingh B, Valan Arasu A. A detailed review on heat transfer rate, supercooling, thermal stability and reliability of nanoparticle dispersed organic phase change material for low-temperature applications. *Mater Today Energy* 2020; **16**: 100408.

35 Zhao Y, Zhang X, Xu X, *et al.* Research progress in nucleation and supercooling induced by phase change materials. *J Energy Storage* 2020; **27**: 101156.

36 Shamseddine I, Pennec F, Biwole P, *et al.* Supercooling of phase change materials: A review. *Renew Sustain Energy Rev* 2022; **158**: 112172.

37 Hassanpouryouzband A, Joonaki E, Vasheghani Farahani M, *et al.* Gas hydrates in sustainable chemistry. *Chem Soc Rev* 2020; **49**: 5225–5309.

38 Chalmers B. *Principles of Solidification*. *Applied Solid State Physics*. Boston: Springer, 1964. 161–170.

39 Orava J, Hewak DW, Greer AL. Fragile-to-strong crossover in supercooled liquid Ag-In-Sb-Te studied by ultrafast calorimetry. *Adv Funct Mater* 2015; **25**: 4851–4858.

40 Le Gallo M, Sebastian A. An overview of phase-change memory device physics. *J Phys D-Appl Phys* 2020; **53**: 213002.

41 Mullin JW, Raven KD. Nucleation in agitated solutions. *Nature* 1961; **190**: 251.

42 Cui H, Wang P, Yang H, *et al.* Enhancing the heat transfer and photothermal conversion of salt hydrate phase change material for efficient solar energy utilization. *J Energy Storage* 2022; **49**: 104130.

43 Kubota N, Fujisawa Y, Tadaki T. Effect of volume on the supercooling temperature for primary nucleation of

potassium nitrate from aqueous solution. *J Cryst Growth* 1998; **89**: 545–552.

44 Lopez R, Haynes TE, Boatner LA, *et al.* Size effects in the structural phase transition of VO_2 nanoparticles. *Phys Rev B* 2002; **65**: 224113.

45 Mollova A, Androsch R, Mileva D, *et al.* Effect of supercooling on crystallization of polyamide 11. *Macromolecules* 2013; **46**: 828–835.

46 Safari A, Saidur R, Sulaiman FA, *et al.* A review on supercooling of phase change materials in thermal energy storage systems. *Renew Sustain Energy Rev* 2017; **70**: 905–919.

47 Taylor RA, Tsafnat N, Washer A. Experimental characterisation of sub-cooling in hydrated salt phase change materials. *Appl Thermal Eng* 2016; **93**: 935–938.

48 Solomon GR, Karthikeyan S, Velraj R. Sub cooling of PCM due to various effects during solidification in a vertical concentric tube thermal storage unit. *Appl Thermal Eng* 2013; **52**: 505–511.

49 Oike H, Suda M, Kamitani M, *et al.* Size effects on supercooling phenomena in strongly correlated electron systems: $IrTe_2$ and θ-$(BEDT\text{-}TTF)_2RbZn(SCN)_4$. *Phys Rev B* 2018; **97**: 085102.

50 Telkes M. Nucleation of supersaturated inorganic salt solutions. *Ind Eng Chem* 1952; **44**: 1308–1310.

51 Lane GA. Phase change materials for energy storage nucleation to prevent supercooling. *Sol Energy Mater Sol Cells* 1992; **27**: 135–160.

52 Li X, Zhou Y, Nian H, *et al.* Phase change behavior of latent heat storage media based on calcium chloride hexahydrate composites containing strontium chloride hexahydrate and oxidation expandable graphite. *Appl Thermal Eng* 2016; **102**: 38–44.

53 Zhang Y, Zhang X, Xu X, *et al.* Preparation and characterization of sodium sulfate pentahydrate/sodium pyrophosphate composite phase change energy storage materials. *J Mol Liquids* 2019; **280**: 360–366.

54 Mao J, Dong X, Hou P, *et al.* Preparation research of novel composite phase change materials based on sodium acetate trihydrate. *Appl Thermal Eng* 2017; **118**: 817–825.

55 Mao J, Hou P, Liu R, *et al.* Preparation and thermal properties of SAT-CMC-DSP/EG composite as phase change material. *Appl Thermal Eng* 2017; **119**: 585–592.

56 Li X, Zhou Y, Nian H, *et al.* Preparation and thermal energy storage studies of $CH_3COONa{\cdot}3H_2O$–KCl composites salt system with enhanced phase change performance. *Appl Thermal Eng* 2016; **102**: 708–715.

57 Cui W, Yuan Y, Sun L, *et al.* Experimental studies on the supercooling and melting/freezing characteristics of nano-copper/sodium acetate trihydrate composite phase change materials. *Renew Energy* 2016; **99**: 1029–1037.

58 Fashandi M, Leung SN. Sodium acetate trihydrate-chitin nanowhisker nanocomposites with enhanced phase change performance for thermal energy storage. *Sol Energy Mater Sol Cells* 2018; **178**: 259–265.

59 Hu P, Lu DJ, Fan XY, *et al.* Phase change performance of sodium acetate trihydrate with AlN nanoparticles and CMC. *Sol Energy Mater Sol Cells* 2011; **95**: 2645–2649.

60 Liu Y, Yang Y. Use of nano-α-Al_2O_3 to improve binary eutectic hydrated salt as phase change material. *Sol Energy Mater Sol Cells* 2017; **160**: 18–25.

61 Liu Y, Liu W, Zhang S, *et al.* Preparation and characterization of new nano-particle mixed as thermal storage material. *Appl Thermal Eng* 2019; **163**: 114386.

62 Xie N, Niu J, Wu T, *et al.* Fabrication and characterization of $CaCl_2{\cdot}6H_2O$ composite phase change material in the presence of Cs_xWO_3 nanoparticles. *Sol Energy Mater Sol Cells* 2019; **200**: 110034.

63 Zhang XJ, Wu P, Qiu LM, *et al.* Analysis of the nucleation of nanofluids in the ice formation process. *Energy Convers Manage* 2010; **51**: 130–134.

64 Yang Z, Yang Z, Li J, *et al.* Design of diatomite-based hydrated salt composites with low supercooling degree and enhanced heat transfer for thermal energy storage. *Int J Energy Res* 2019; **43**: 7058–7074.

65 Wang Y, Cao L, Zhang D. Overcoming the supercooling of hydrated salts: Three-dimensional graphene composite PCMs. *Micro & Nano Lett* 2018; **13**: 849–852.

66 Cui W, Jia L, Chen Y, *et al.* Supercooling of water controlled by nanoparticles and ultrasound. *Nanoscale Res Lett*

2018; **13**: 145.

67 Marks S. An investigation of the thermal energy storage capacity of Glauber's salt with respect to thermal cycling. *Sol Energy* 1980; **25**: 255–258.

68 Bao X, Yang H, Xu X, *et al.* Development of a stable inorganic phase change material for thermal energy storage in buildings. *Sol Energy Mater Sol Cells* 2020; **208**: 110420.

69 Shahbaz K, AlNashef IM, Lin RJT, *et al.* A novel calcium chloride hexahydrate-based deep eutectic solvent as a phase change materials. *Sol Energy Mater Sol Cells* 2016; **155**: 147–154.

70 Cabeza LF, Svensson G, Hiebler S, *et al.* Thermal performance of sodium acetate trihydrate thickened with different materials as phase change energy storage material. *Appl Thermal Eng* 2003; **23**: 1697–1704.

71 Efimova A, Pinnau S, Mischke M, *et al.* Development of salt hydrate eutectics as latent heat storage for air conditioning and cooling. *Thermochim Acta* 2014; **575**: 276–278.

72 Tang W, Kardani O, Cui H. Robust evaluation of self-healing efficiency in cementitious materials—A review. *Constr Build Mater* 2015; **81**: 233–247.

73 Lan XZ, Tan ZC, Shi Q, *et al.* A novel gelling method for stabilization of phase change material $Na_2HPO_4{\cdot}12H_2O$ with sodium alginate grafted sodium acrylate. *Thermochim Acta* 2007; **463**: 18–20.

74 Liu Y, Yu K, Gao X, *et al.* Enhanced thermal properties of hydrate salt/poly (acrylate sodium) copolymer hydrogel as form-stable phase change material via incorporation of hydroxyl carbon nanotubes. *Sol Energy Mater Sol Cells* 2020; **208**: 110387.

75 Liu Y, Yang Y, Li S. Graphene oxide modified hydrate salt hydrogels: Form-stable phase change materials for smart thermal management. *J Mater Chem A* 2016; **4**: 18134–18143.

76 Karimineghlani P, Emmons E, Green MJ, *et al.* A temperature-responsive poly(vinyl alcohol) gel for controlling fluidity of an inorganic phase change material. *J Mater Chem A* 2017; **5**: 12474–12482.

77 Rathore PKS, Shukla SK. Enhanced thermophysical properties of organic PCM through shape stabilization for thermal energy storage in buildings: A state of the art review. *Energy Buildings* 2021; **236**: 110799.

78 Fu L, Wang Q, Ye R, *et al.* A calcium chloride hexahydrate/expanded perlite composite with good heat storage and insulation properties for building energy conservation. *Renew Energy* 2017; **114**: 733–743.

79 Rao Z, Xu T, Liu C, *et al.* Experimental study on thermal properties and thermal performance of eutectic hydrated salts/expanded perlite form-stable phase change materials for passive solar energy utilization. *Sol Energy Mater Sol Cells* 2018; **188**: 6–17.

80 Rathore PKS, Shukla S. Improvement in thermal properties of PCM/Expanded vermiculite/expanded graphite shape stabilized composite PCM for building energy applications. *Renew Energy* 2021; **176**: 295–304.

81 Xie N, Luo J, Li Z, *et al.* Salt hydrate/expanded vermiculite composite as a form-stable phase change material for building energy storage. *Sol Energy Mater Sol Cells* 2019; **189**: 33–42.

82 Liu J, Zhu C, Liang W, *et al.* Experimental investigation on micro-scale phase change material based on sodium acetate trihydrate for thermal storage. *Sol Energy* 2019; **193**: 413–421.

83 Xie N, Niu J, Zhong Y, *et al.* Development of polyurethane acrylate coated salt hydrate/diatomite form-stable phase change material with enhanced thermal stability for building energy storage. *Constr Build Mater* 2020; **259**: 119714.

84 Xu T, Wu F, Zou T, *et al.* Development of diatomite-based shape-stabilized composite phase change material for use in floor radiant heating. *J Mol Liquids* 2022; **348**: 118372.

85 Mohseni E, Tang W, Khayat KH, *et al.* Thermal performance and corrosion resistance of structural-functional concrete made with inorganic PCM. *Constr Build Mater* 2020; **249**: 118768.

86 Álvarez-Bermúdez O, Adam-Cervera I, Aguado-Hernández A, *et al.* Magnetic polyurethane microcarriers from nanoparticle-stabilized emulsions for thermal energy storage. *ACS Sustain Chem Eng* 2020; **8**: 17956–17966.

87 Liu Z, Chen Z, Yu F. Preparation and characterization of microencapsulated phase change materials containing inorganic hydrated salt with silica shell for thermal energy storage. *Sol Energy Mater Sol Cells* 2019; **200**: 110004.

88 Zhang Z, Lian Y, Xu X, *et al.* Synthesis and characterization of microencapsulated sodium sulfate decahydrate as phase

change energy storage materials. *Appl Energy* 2019; **255**: 113830.

89 Li M, Wang W, Zhang Z, *et al.* Monodisperse $Na_2SO_4{\cdot}10H_2O@SiO_2$ microparticles against supercooling and phase separation during phase change for efficient energy storage. *Ind Eng Chem Res* 2017; **56**: 3297–3308.

90 Liu C, Wang C, Li Y, *et al.* Preparation and characterization of sodium thiosulfate pentahydrate/silica microencapsulated phase change material for thermal energy storage. *RSC Adv* 2017; **7**: 7238–7249.

91 Huang J, Wang T, Zhu P, *et al.* Preparation, characterization, and thermal properties of the microencapsulation of a hydrated salt as phase change energy storage materials. *Thermochim Acta* 2013; **557**: 1–6.

92 Purohit BK, Sistla VS. Inorganic salt hydrate for thermal energy storage application: A review. *Energy Storage* 2021; **3**: e212.

93 Dixit P, Reddy VJ, Parvate S, *et al.* Salt hydrate phase change materials: Current state of art and the road ahead. *J Energy Storage* 2022; **51**: 104360.

94 Li Y, Li C, Lin N, *et al.* Review on tailored phase change behavior of hydrated salt as phase change materials for energy storage. *Mater Today Energy* 2021; **22**: 100866.

95 Zheng M, Xie C, Liu J, *et al.* Composite hydrate salt Na_2 $HPO_4{\cdot}12H_2$ O–Na_2 $SO_4{\cdot}10H_2O$ and its thermal storage properties. *Emerging Mater Res* 2019; **8**: 68–76.

96 Shahid UB, Abdala A. A critical review of phase change material composite performance through Figure-of-Merit analysis: Graphene vs. Boron Nitride. *Energy Storage Mater* 2021; **34**: 365–387.

97 Liu L, Su D, Tang Y, *et al.* Thermal conductivity enhancement of phase change materials for thermal energy storage: A review. *Renew Sustain Energy Rev* 2016; **62**: 305–317.

98 Wu S, Yan T, Kuai Z, *et al.* Thermal conductivity enhancement on phase change materials for thermal energy storage: A review. *Energy Storage Mater* 2020; **25**: 251–295.

99 Tian H, Du L, Wei X, *et al.* Enhanced thermal conductivity of ternary carbonate salt phase change material with Mg particles for solar thermal energy storage. *Appl Energy* 2017; **204**: 525–530.

100 Sharshir SW, El-Shafai NM, Ibrahim MM, *et al.* Effect of copper oxide/cobalt oxide nanocomposite on phase change material for direct/indirect solar energy applications: Experimental investigation. *J Energy Storage* 2021; **38**: 102526.

101 Deng Y, Li J, Qian T, *et al.* Thermal conductivity enhancement of polyethylene glycol/expanded vermiculite shape-stabilized composite phase change materials with silver nanowire for thermal energy storage. *Chem Eng J* 2016; **295**: 427–435.

102 Petersen EM, Rao RG, Vance BC, *et al.* SiO_2/SiC supports with tailored thermal conductivity to reveal the effect of surface temperature on Ru-catalyzed CO_2 methanation. *Appl Catal B-Environ* 2021; **286**: 119904.

103 Kim HG, Qudoos A, Jeon IK, *et al.* Assessment of PCM/SiC-based composite aggregate in concrete: Energy storage performance. *Constr Build Mater* 2020; **258**: 119637.

104 Guerra V, Wan C, McNally T. Thermal conductivity of 2D nano-structured boron nitride (BN) and its composites with polymers. *Prog Mater Sci* 2019; **100**: 170–186.

105 Cheng P, Chen X, Gao H, *et al.* Different dimensional nanoadditives for thermal conductivity enhancement of phase change materials: Fundamentals and applications. *Nano Energy* 2021; **85**: 105948.

106 Zhang L, Zhou K, Wei Q, *et al.* Thermal conductivity enhancement of phase change materials with 3D porous diamond foam for thermal energy storage. *Appl Energy* 2019; **233-234**: 208–219.

107 Touloukian Y, Makita T. Thermophysical properties of matter-the TPRC data series. Volume 6. Specific heat-nonmetallic liquids and gases. Technical Report. 1970. file:///C:/Users/Administrator/Downloads/ADA951940.pdf.

108 Chen G. *Nanoscale Energy Transport and Conversion: A Parallel Treatment of Electrons, Molecules, Phonons, and Photons*. Oxford: Oxford University Press, 2005.

109 Nika DL, Pokatilov EP, Askerov AS, *et al.* Phonon thermal conduction in graphene: Role of Umklapp and edge roughness scattering. *Phys Rev B* 2009; **79**: 155413.

110 Yuan K, Shi J, Aftab W, *et al.* Engineering the thermal conductivity of functional phase-change materials for heat energy conversion, storage, and utilization. *Adv Funct Mater* 2020; **30**: 1904228.

111 Xiao Q, Zhang M, Fan J, *et al.* Thermal conductivity enhancement of hydrated salt phase change materials employing copper foam as the supporting material. *Sol Energy Mater Sol Cells* 2019; **199**: 91–98.

112 Wu F, Lin Z, Xu T, *et al.* Development and thermal properties of a novel sodium acetate trihydrate-Acetamide-micron/nano aluminum nitride composite phase change material. *Mater Des* 2020; **196**: 109113.

113 Dannemand M, Johansen JB, Furbo S. Solidification behavior and thermal conductivity of bulk sodium acetate trihydrate composites with thickening agents and graphite. *Sol Energy Mater Sol Cells* 2016; **145**: 287–295.

114 Li X, Zhou Y, Nian H, *et al.* Advanced nanocomposite phase change material based on calcium chloride hexahydrate with aluminum oxide nanoparticles for thermal energy storage. *Energy Fuels* 2017; **31**: 6560–6567.

115 Tang A, Chen W, Shao X, *et al.* Experimental investigation of aluminum nitride/carbon fiber-modified composite phase change materials for battery thermal management. *Intl J Energy Res* 2022; **46**: 12737–12757.

116 He Y, Zhang N, Yuan Y, *et al.* Improvement of supercooling and thermal conductivity of the sodium acetate trihydrate for thermal energy storage with α-Fe_2O_3 as addictive. *J Therm Anal Calorim* 2018; **133**: 859–867.

117 Tie J, Liu X, Tie S, *et al.* Packing and properties of composite phase change energy storage materials based on SiC nanowires and $Na_2SO_4{\cdot}10H_2O$. *J Therm Anal Calorim* 2019; **139**: 855–862.

118 Mehrali M, ten Elshof JE, Shahi M, *et al.* Simultaneous solar-thermal energy harvesting and storage via shape stabilized salt hydrate phase change material. *Chem Eng J* 2021; **405**: 126624.

119 Cui K, Liu L, Ma F, *et al.* Enhancement of thermal conductivity of $Ba(OH)_2{\cdot}8H_2$ O phase change material by graphene nanoplatelets. *Mater Res Express* 2018; **5**: 065522.

120 Fu W, Lu Y, Zhang R, *et al.* Developing $NaAc{\cdot}3H_2O$-based composite phase change material using glycine as temperature regulator and expanded graphite as supporting material for use in floor radiant heating. *J Mol Liquids* 2020; **317**: 113932.

121 Xiao Q, Yuan W, Li L, *et al.* Fabrication and characteristics of composite phase change material based on $Ba(OH)_2{\cdot}8H_2O$ for thermal energy storage. *Sol Energy Mater Sol Cells* 2018; **179**: 339–345.

122 Li TX, Wu DL, He F, *et al.* Experimental investigation on copper foam/hydrated salt composite phase change material for thermal energy storage. *Int J Heat Mass Transfer* 2017; **115**: 148–157.

123 Zou T, Fu W, Liang X, *et al.* Preparation and performance of modified calcium chloride hexahydrate composite phase change material for air-conditioning cold storage. *Int J Refrigeration* 2018; **95**: 175–181.

124 Fu W, Zou T, Liang X, *et al.* Thermal properties and thermal conductivity enhancement of composite phase change material using sodium acetate trihydrate–urea/expanded graphite for radiant floor heating system. *Appl Thermal Eng* 2018; **138**: 618–626.

125 Jin X, Xiao Q, Xu T, *et al.* Thermal conductivity enhancement of a sodium acetate trihydrate–potassium chloride–urea/expanded graphite composite phase–change material for latent heat thermal energy storage. *Energy Buildings* 2021; **231**: 110615.

126 Fu W, Zou T, Liang X, *et al.* Preparation and properties of phase change temperature-tuned composite phase change material based on sodium acetate trihydrate-urea/fumed silica for radiant floor heating system. *Appl Thermal Eng* 2019; **162**: 114253.

127 Fang Y, Ding Y, Tang Y, *et al.* Thermal properties enhancement and application of a novel sodium acetate trihydrate-formamide/expanded graphite shape-stabilized composite phase change material for electric radiant floor heating. *Appl Thermal Eng* 2019; **150**: 1177–1185.

128 Zeinelabdein R, Omer S, Gan G. Critical review of latent heat storage systems for free cooling in buildings. *Renew Sustain Ener Rev* 2018; **82**: 2843–2868.

129 Li G, Zhang B, Li X, *et al.* The preparation, characterization and modification of a new phase change material: $CaCl_2{\cdot}6H_2O$–$MgCl_2{\cdot}6H_2O$ eutectic hydrate salt. *Sol Energy Mater Sol Cells* 2014; **126**: 51–55.

130 Marín PE, Ushak S, de Gracia A, *et al.* Assessing corrosive behaviour of commercial phase change materials in the 21–25°C temperature range. *J Energy Storage* 2020; **32**: 101711.

131 Moreno P, Miró L, Solé A, *et al.* Corrosion of metal and metal alloy containers in contact with phase change materials

(PCM) for potential heating and cooling applications. *Appl Energy* 2014; **125**: 238–245.

132 Solé A, Miró L, Barreneche C, *et al.* Corrosion test of salt hydrates and vessel metals for thermochemical energy storage. *Energy Procedia* 2014; **48**: 431–435.

133 Calabrese L, Brancato V, Palomba V, *et al.* An experimental study on the corrosion sensitivity of metal alloys for usage in PCM thermal energy storages. *Renew Energy* 2019; **138**: 1018–1027.

134 Honcova P, Pilar R, Danielik V, *et al.* Suppressing supercooling in magnesium nitrate hexahydrate and evaluating corrosion of aluminium alloy container for latent heat storage application. *J Therm Anal Calorim* 2017; **129**: 1573–1581.

135 Danielik V, Šoška P, Felgerová K, *et al.* The corrosion of carbon steel in nitrate hydrates used as phase change materials. *Mater Corrosion* 2017; **68**: 416–422.

136 Zhao T, Zheng M, Munis A, *et al.* Corrosion behaviours of typical metals in molten hydrate salt of $Na_2HPO_4{\cdot}12H_2O$–$Na_2SO_4{\cdot}10H_2O$ for thermal energy storage. *Corrosion Eng Sci Tech* 2019; **54**: 379–388.

137 Solé A, Miró L, Barreneche C, *et al.* Corrosion of metals and salt hydrates used for thermochemical energy storage. *Renew Energy* 2015; **75**: 519–523.

138 Devanuri JK, Gaddala UM, Kumar V. Investigation on compatibility and thermal reliability of phase change materials for low-temperature thermal energy storage. *Mater Renew Sustain Energy* 2020; **9**: 24.

139 Cabeza LF, Illa J, Roca J, *et al.* Middle term immersion corrosion tests on metal-salt hydrate pairs used for latent heat storage in the 32 to 36°C temperature range. *Werkstoffe und Korrosion* 2001; **52**: 748.

140 Cabeza LF, Illa J, Roca J, *et al.* Immersion corrosion tests on metal-salt hydrate pairs used for latent heat storage in the 32 to 36°C temperature range. *Mater Corrosion* 2001; **52**: 140–146.

141 Di Franco F, Zaffora A, Megna B, *et al.* Heterogeneous crystallization of zinc hydroxystannate on galvanized steel for enhancing the bond strength at the rebar/concrete interface. *Chem Eng J* 2021; **405**: 126943.

142 Farid MM, Khudhair AM, Razack SAK, *et al.* A review on phase change energy storage: materials and applications. *Energy Convers Manage* 2004; **45**: 1597–1615.

143 Ding Z, Wu W, Chen Y, *et al.* Dynamic simulation and parametric study of solar water heating system with phase change materials in different climate zones. *Sol Energy* 2020; **205**: 399–408.

144 Kılıçkap S, El E, Yıldız C. Investigation of the effect on the efficiency of phase change material placed in solar collector tank. *Thermal Sci Eng Prog* 2018; **5**: 25–31.

145 Douvi E, Pagkalos C, Dogkas G, *et al.* Phase change materials in solar domestic hot water systems: A review. *Int J Thermofluids* 2021; **10**: 100075.

146 Madhankumar S, Viswanathan K, Wu W, *et al.* Analysis of indirect solar dryer with PCM energy storage material: Energy, economic, drying and optimization. *Sol Energy* 2023; **249**: 667–683.

147 Babar OA, Arora VK, Nema PK, *et al.* Effect of PCM assisted flat plate collector solar drying of green chili on retention of bioactive compounds and control of aflatoxins development. *Sol Energy* 2021; **229**: 102–111.

148 Albdour SA, Haddad Z, Sharaf OZ, *et al.* Micro/nano-encapsulated phase-change materials (ePCMs) for solar photothermal absorption and storage: Fundamentals, recent advances, and future directions. *Prog Energy Combust Sci* 2022; **93**: 101037.

149 Ma T, Yang H, Zhang Y, *et al.* Using phase change materials in photovoltaic systems for thermal regulation and electrical efficiency improvement: A review and outlook. *Renew Sustain Energy Rev* 2015; **43**: 1273–1284.

150 Mardiana-Idayu A, Riffat SB. Review on heat recovery technologies for building applications. *Renew Sustain Energy Rev* 2012; **16**: 1241–1255.

151 Sonnick S, Erlbeck L, Gaedtke M, *et al.* Passive room conditioning using phase change materials: Demonstration of a long-term real size experiment. *Int J Energy Res* 2020; **44**: 7047–7056.

152 Sonnick S, Erlbeck L, Schlachter K, *et al.* Temperature stabilization using salt hydrate storage system to achieve thermal comfort in prefabricated wooden houses. *Energy Buildings* 2018; **164**: 48–60.

153 de Gracia A, Rincón L, Castell A, *et al.* Life cycle assessment of the inclusion of phase change materials (PCM) in

experimental buildings. *Energy Buildings* 2010; **42**: 1517–1523.

154 Mukhamet T, Kobeyev S, Nadeem A, *et al.* Ranking PCMs for building façade applications using multi-criteria decision-making tools combined with energy simulations. *Energy* 2021; **215**: 119102.

155 Barla M, Di Donna A. Energy tunnels: Concept and design aspects. *Underground Space* 2018; **3**: 268–276.

156 Fadejev J, Simson R, Kurnitski J, *et al.* A review on energy piles design, sizing and modelling. *Energy* 2017; **122**: 390–407.

157 Makasis N, Narsilio GA. Energy diaphragm wall thermal design: The effects of pipe configuration and spacing. *Renew Energy* 2020; **154**: 476–487.

158 Alavy M, Peiris M, Wang J, *et al.* Assessment of a novel phase change material-based thermal caisson for geothermal heating and cooling. *Energy Convers Manage* 2021; **234**: 113928.

159 Cao Z, Zhang G, Liu Y, *et al.* Influence of backfilling phase change material on thermal performance of precast high-strength concrete energy pile. *Renew Energy* 2022; **184**: 374–390.

160 Mousa MM, Bayomy AM, Saghir MZ. Long-term performance investigation of a GSHP with actual size energy pile with PCM. *Appl Thermal Eng* 2022; **210**: 118381.

161 Du T, Li Y, Bao X, *et al.* Thermo-mechanical performance of a phase change energy pile in saturated sand. *Symmetry* 2020; **12**: 1781.

162 Bao X, Shi J, Chen G, *et al.* Laboratory tests and numerical simulation of the thermal-mechanical response of a fiber-reinforced phase change concrete pile. *Appl Sci* 2023; **13**: 11853.

163 Bao X, Qi X, Cui H, *et al.* Comparison study on the performance of a novel and traditional energy piles by laboratory tests. *Symmetry* 2021; **13**: 1958.

164 Han C, Shen Y, Chen K, *et al.* Characteristics and energy performance of novel MicroPCM C50 energy pile in cooling mode. *Energy Buildings* 2022; **274**: 112442.

165 Shahidi S, Hajialilue-Bonab M, Tohidvand HR, *et al.* Experimental investigation on the efficiency of the phase change materials for enhancing the thermal performance of energy piles in sandy soils. *Energy Buildings* 2023; **298**: 113544.

166 Warner J, Liu X, Shi L, *et al.* A novel shallow bore ground heat exchanger for ground source heat pump applications—Model development and validation. *Appl Thermal Eng* 2020; **164**: 114460.

167 Zhang M, Liu X, Biswas K, *et al.* A three-dimensional numerical investigation of a novel shallow bore ground heat exchanger integrated with phase change material. *Appl Thermal Eng* 2019; **162**: 114297.

168 Cao Z, Zhang G, Wu Y, *et al.* Energy storage potential analysis of phase change material (PCM) energy storage units based on tunnel lining ground heat exchangers. *Appl Thermal Eng* 2023; **235**: 121403.

169 Dong Z, Cui H, Tang W, *et al.* Development of hollow steel ball macro-encapsulated PCM for thermal energy storage concrete. *Materials* 2016; **9**: 59.

170 Cui H, Tang W, Qin Q, *et al.* Development of structural-functional integrated energy storage concrete with innovative macro-encapsulated PCM by hollow steel ball. *Appl Energy* 2017; **185**: 107–118.

171 Cui H, Zou J, Gong Z, *et al.* Study on the thermal and mechanical properties of steel fibre reinforced PCM-HSB concrete for high performance in energy piles. *Constr Build Mater* 2022; **350**: 128822.